2

South Asian monsoon

B. N. Goswami

2.1 INTRODUCTION

2.1.1 South Asian summer monsoon and active/break cycles

As the word "monsoon" (derived from an Arabic word meaning "seasons") indicates, the South Asian (SA) summer monsoon is part of an annually reversing wind system (Figure 2.1c, d) (Ramage, 1971; Rao, 1976). The winds at low levels during the summer monsoon season are characterized by the strongest westerlies anywhere in the tropics at 850 hPa over the Arabian Sea, known as the low-level westerly jet (LLJ) (Figure 2.1d), and a large-scale cyclonic vorticity extending from the north Bay of Bengal (BoB) to western India known as the monsoon trough (Figure 2.1d) (Rao, 1976). The easterly jet (Figure 2.1f) centered around 5°N and the Tibetan anticyclone centered around 30°N are important features of upper-level winds over the monsoon region during northern summer. Millions of inhabitants of the region, however, attach much greater importance to the associated seasonal changes of rainfall. Wet summers and dry winters (Figure 2.1a, b) associated with the seasonal changes of low-level winds are crucial for agricultural production and the economy of the region. The monsoon, or the seasonal changes of winds and rainfall, in the region could be interpreted as a result of northward seasonal migration of the east–west oriented precipitation belt (Tropical Convergence Zone, TCZ) from the southern hemisphere in winter to the northern hemisphere in summer (Gadgil, 2003). The largest northward excursion of the rain belt takes place over the Indian monsoon region where it moves from a mean position of about 5°S in winter (Figure 2.1a) to about 20°N in northern summer (Figure 2.1b) (Waliser and Gautier, 1993). In the upper atmosphere (200 hPa), the equatorial easterlies are weak and confined between 5°N and 10°S while the subtropical westerlies intrude all the way to 10°N during northern winter (Figure 2.1e). The subtropical westerlies recede to north of 30°N during northern summer and a strong easterly jet

W. K. M. Lau and D. E. Waliser (Editors), *Intraseasonal Variability in the Atmosphere–Ocean Climate System* (Second Edition).

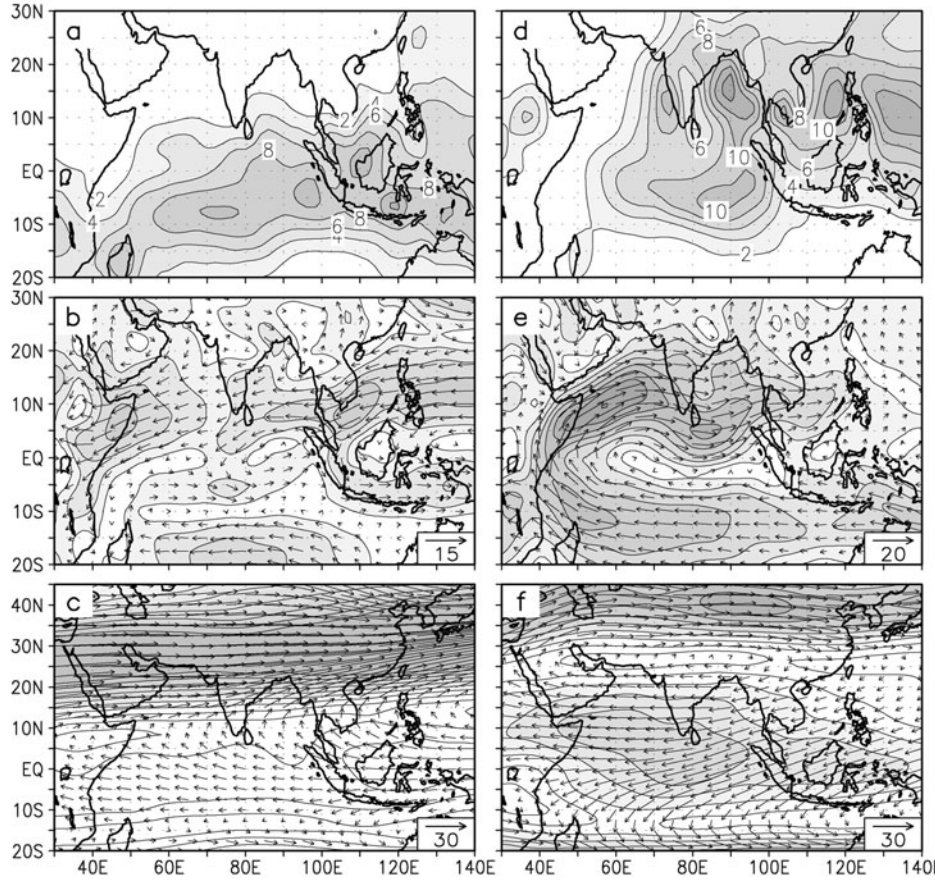

Figure 2.1. Climatological mean precipitation (mm/day) based on CMAP during (a) boreal winter (DJF) and (b) summer (JJAS). (c) and (d) Same as (a) and (b) but for winds ($m\,s^{-1}$) at 850 hPa based on NCEP reanalysis. The contour interval for isotachs is $2\,m\,s^{-1}$ with the minimum contour being 2. (e) and (f) Similar to (c) and (d) but for winds at 200 hPa. The contour interval for isotachs is $5\,m\,s^{-1}$ with the minimum contour being 5. For better depiction of the subtropical westerly jetstream in winter and the Tibetan anticyclone in summer, a larger meridional domain is used for 200 hPa winds (e) and (f).

characterizes the equatorial upper atmosphere in the region (Figure 2.1f). Year-to-year variation of long-term seasonal mean precipitation over the Indian region is strongly correlated with food production in the region (Parthasarathy *et al.*, 1988; Webster *et al.*, 1998; Abrol and Gadgil, 1999). Extremes in year-to-year variations of long-term mean precipitation manifest themselves in the form of large-scale floods and droughts (Parthasarathy and Mooley, 1978; Shukla, 1987; Mooley and Shukla, 1987) and cause devastating human and economic loss.

The seasonal mean rainfall of approximately $8\,mm\,day^{-1}$ does not pour as a continuous deluge but is punctuated by considerable variations within the season.

In addition to the day-to-day fluctuations of weather (e.g., lows and depressions) with timescales of 5–7 days (also known as synoptic disturbances), a characteristic feature of monsoon rainfall is the prolonged spells of dry and wet conditions often lasting for 2–3 weeks. Examples of such spells can be seen in the time series of rainfall averaged over central India between June 1 and September 30, 1972, 1994, and 2002 (Figure 2.2). As seen during 1972, the evolution of rainfall over the season generally goes through extended periods of above-normal conditions (wet spells) followed by extended periods of below-normal conditions (dry spells). Extended above-normal rain spells can be seen to represent epochs when the monsoon was vigorous or active while the dry spells represent periods when the monsoon took a break from its activity (Ramamurthy, 1969; Raghavan, 1973) and hence are known as active and break conditions, respectively. Frequent or prolonged breaks within the monsoon season, as in the case of 1972 and 2002 (Figure 2.2), lead to drought conditions and adversely affect agricultural production (Gadgil, 1995; Webster *et al*., 1998). Similarly, the above-normal seasonal rainfall in 1994 was a result of the occurrence of more active spells and an absence of extended break spells within the season. Thus, frequency of occurrence of active and break spells influences seasonal mean rainfall and hence agricultural production. For example, long breaks in critical growth periods of agricultural crops also lead to substantially reduced yields (Gadgil and Rao, 2000). As a consequence of their influence in agricultural production and water resources, considerable attention has been paid toward understanding the nature of monsoon breaks and the possible mechanism responsible for them. In fact, the earliest reference to monsoon breaks was made more than a century ago by Blanford (1886), where he refers to the periods between two active spells as intervals of droughts. Using upper-air data over the Indian continent and its neighborhood, large-scale circulation changes associated with active and break conditions have been identified (Ramamurthy, 1969; Raghavan, 1973; Krishnamurti and Bhalme, 1976; Sikka, 1980; Alexander *et al*., 1978). The active (break) condition is generally associated with an increase (decrease) of cyclonic vorticity and decrease (increase) of surface pressure over the central Indian monsoon trough region and strengthening (weakening) of the LLJ. Movement of the low-level trough (monsoon trough) to the foothills of the Himalayas during break conditions have been recorded (Ramamurthy, 1969; Raghavan, 1973; Krishnamurti and Bhalme, 1976; Sikka, 1980; Alexander *et al*., 1978). Weakening of the Tibetan anticyclone in the upper atmosphere and extension of a large-amplitude trough in midlatitude westerlies up to northern Indian latitudes are also associated with monsoon breaks (Ramaswamy, 1962).

The dry and wet spells of active and break conditions represent subseasonal or intraseasonal variation (ISV) of the monsoon with timescales longer than synoptic variability (1–10 days) but shorter than a season. Studies have also shown (Dakshinamurthy and Keshavamurthy, 1976; Alexander *et al*., 1978) certain preferred periodicities are associated with the monsoon ISV indicating that certain oscillations (intraseasonal oscillations, or ISOs) are involved in generating ISV. Early studies on monsoon ISV that manifest in active and break cycles were based on station rainfall data and soundings from a few upper-air stations. The availability

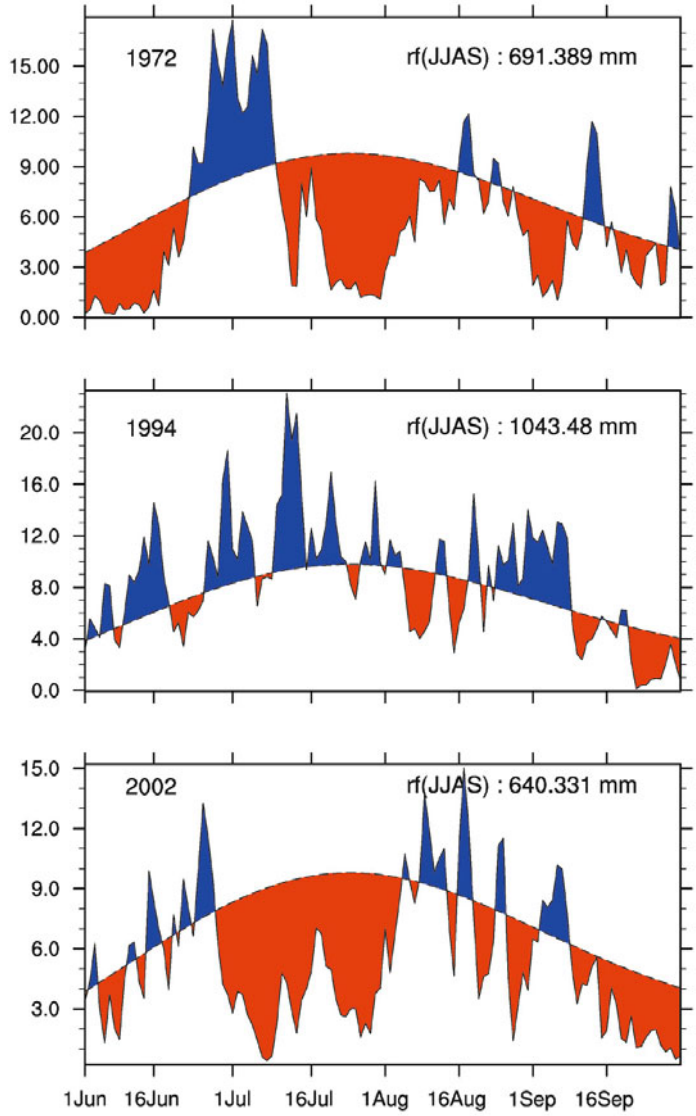

Figure 2.2. Daily rainfall (mm day^{-1}) averaged over 72.5°E–85.5°E and 10.5°N–25.5°N based on high-resolution daily gridded rainfall data (IMD) over the Indian subcontinent during the summer monsoon season for 3 years: 1972, 1994, and 2002. Departures from the mean annual cycle (shown as the envelope) are shaded. Seasonal mean rainfall for each year is also shown in the top-right corners.

of daily satellite cloudiness data and operational analysis in the mid 1970s with global coverage brought new insight regarding the large-scale spatial structure and relationship between the convection and circulation of monsoon ISV. Progress in modeling during the past three decades has also provided new insight regarding the

origin of monsoon ISV. Recently made available gridded daily rainfall data over continental India for more than 50 years (Rajeevan *et al.*, 2006) also helps in bringing out the spatial patterns of anomalies of rainfall associated with different phases of ISV. This dataset has also allowed better delineation of the active and break spells of the Indian monsoon (Rajeevan *et al.* 2010). During this period, we have also learned how monsoon ISOs interact with different scales of motion. At one end of the spectrum, they interact with the annual cycle influencing the seasonal mean, its interannual variability (IAV), and limiting the predictability of the seasonal mean, while at the other end they modulate synoptic activity and cause spatial and temporal clustering of lows and depressions. In this chapter, we attempt to provide a synthesis of the observed spatial and temporal scale of monsoon ISOs, their regional propagation characteristics, relationships with large-scale regional and global circulation, together with a review of theories for their scale selection. The mechanism through which monsoon ISOs influence the seasonal mean and its IAV will also be highlighted. The variety of observations utilized and analysis methodology employed to highlight these different aspects of summer monsoon ISOs are described in the appendix to this chapter (p. 64).

2.1.2 Amplitude and temporal and spatial scales

Distinct from the synoptic disturbances (lows and depressions), the ISOs of monsoons essentially have timescales between 10 and 90 days. In order to get an idea of the amplitude of intraseasonal variability (ISV), it is compared with that of the interannual variability of the seasonal mean and the annual cycle in Figure 2.3. The standard deviation of 10 to 90-day filtered rainfall from GPCP (Figure 2.3a) shows that the amplitude of the ISV is much larger than that of interannual variability of the seasonal mean (Figure 2.3b) and comparable with the amplitude of the seasonal cycle (Figure 2.3c). Thus, the ISV of Asian monsoon rainfall represents a very large–amplitude low-frequency signal. This aspect of monsoon ISV provides some hope for extended range prediction of the active/break spells associated with them (see Section 2.6).

Insight regarding the spatial structure of ISOs and coupling between different variables may be obtained by constructing an index of monsoon ISOs. We construct such an index based on 10 to 90-day bandpass-filtered GPCP precipitation averaged over the box between 70°E–90°E and 15°N–25°N during June 1 and September 30 of each year. The time series normalized by its own standard deviation (2.35 mm day^{-1}) (hereafter referred to as the ISO index) $> +1$ (< -1) represents active (break) conditions as seen from Figure 2.4, where a sample of the ISO index for 10 summer seasons (122 days in each season) is shown.

A lag regression analysis of 10 to 90-day filtered winds from U.S. National Center for Environmental Prediction/National Center for Atmospheric Research (NCEP/NCAR) reanalysis (Kalnay *et al.*, 1996; Kistler *et al.*, 2001) at a number of vertical levels and 10 to 90-day filtered GPCP precipitation with respect to the ISO index brings out the vertical structure and relationship between convection and circulation of the ISV. Simultaneous regressions of GPCP rainfall and 850 hPa

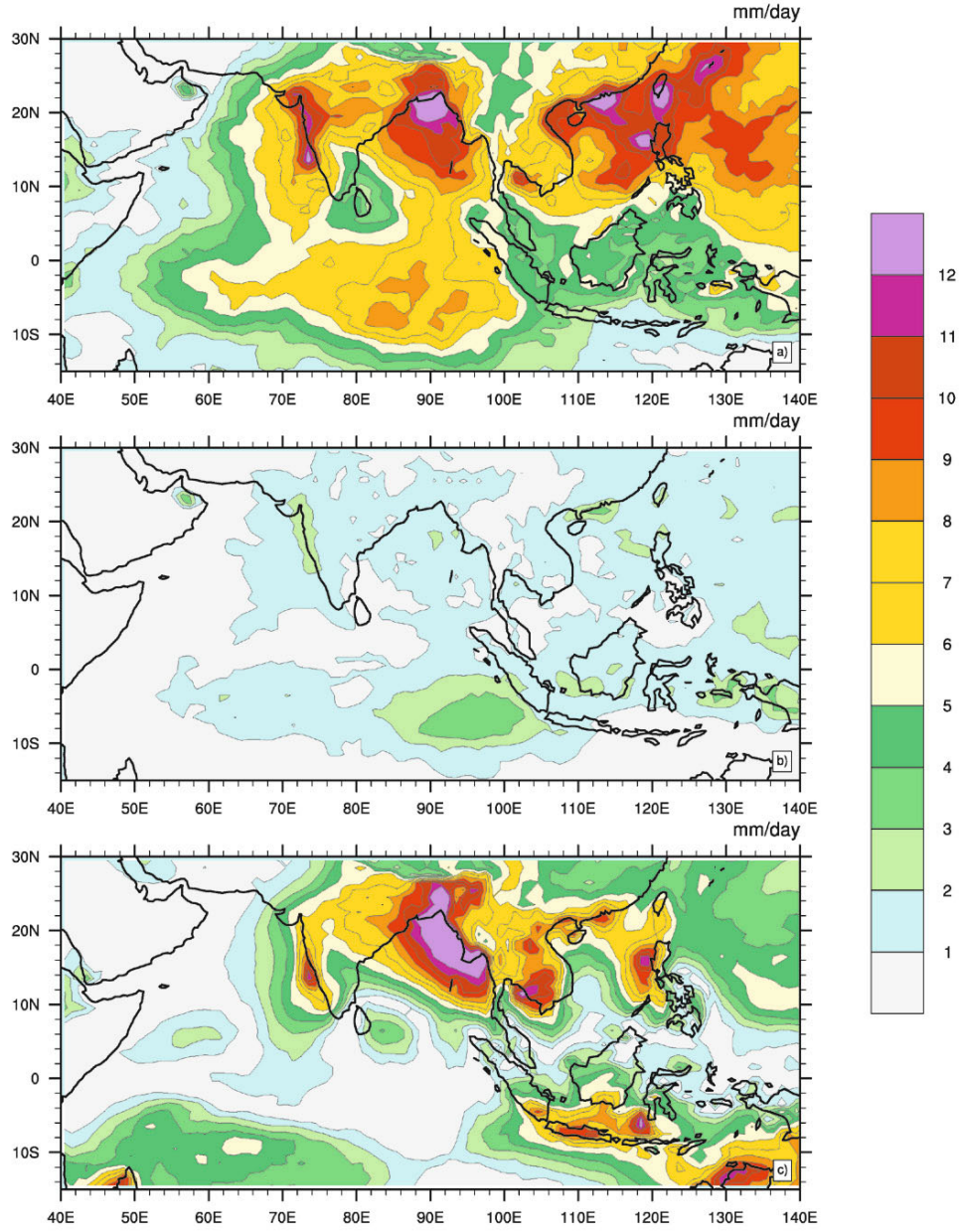

Figure 2.3. (a) Standard deviation of 10 to 90-day filtered GPCP precipitation anomalies (mm/day) based on 1997–2007 JJAS seasons. (b) Standard deviation of IAV of JJAS seasonal mean for the period 1997–2007. (c) Amplitude of the annual cycle. Climatological mean absolute value of the difference between JJAS mean and DJF mean for the 1997–2007 period from GPCP.

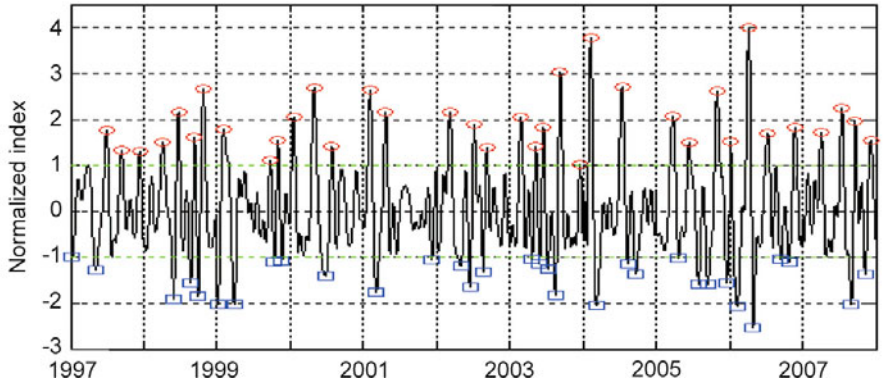

Figure 2.4. Time series of normalized monsoon ISO index between June 1 and September 30 (122 days) for a sample of 11 (1997–2007) summer seasons. The ISO index is defined as 10 to 90-day filtered GPCP rainfall anomaly averaged between 70°E–90°E and 15°N–25°N. The time series is normalized by its own standard deviation. Open circles and squares indicate peaks of active and break conditions, respectively.

winds and those with a lag of 14 days are shown in Figure 2.5a, b. The spatial pattern of precipitation during active and break cycles over the Indian continent corresponds well with active (break) patterns described in other studies (Singh *et al*., 1992; Krishnamurthy and Shukla, 2000; Rajeevan *et al*. 2010). The composite from GPCP within the Indian continent is very similar to that obtained from station data. It also illustrates that monsoon ISV with active/break phases is not confined to the Indian continent but has a much larger spatial scale and is associated with enhanced (decreased) rainfall extending from the western Pacific to the north BoB and central Indian continent. This observation also highlights that ISV during northern summer over the SA monsoon region and ISVs over the East Asian and western North Pacific (EA/WNP) monsoon region are interlinked (see also Chapter 3). One important characteristic of SA monsoon ISV is the north–south dipole in precipitation with active (break) conditions being associated with enhanced (decreased) precipitation over the monsoon trough region and decreased (enhanced) precipitation over the eastern equatorial Indian Ocean (IO) (Goswami and Ajaya Mohan, 2001). Another aspect of the spatial structure of the dominant ISV is a dipole-like structure of opposite sign over the western equatorial Pacific and western North Pacific (Annamalai and Slingo, 2001).

The anomalous meridional circulation associated with active (0 lag) and break (14-day lag) phases are shown in Figure 2.5c, d based on regressions of meridional and vertical velocities with respect to the ISO index averaged between 70°E and 90°E. The low-level wind anomalies associated with ISOs (Figure 2.5a, b) are consistent with a linear response to corresponding precipitation anomalies, indicating that monsoon ISV and active/break conditions are opposite phases of large-scale convectively coupled oscillation. Anomalous Hadley circulation of opposite sign associated with active and break phases shows that regional monsoon Hadley

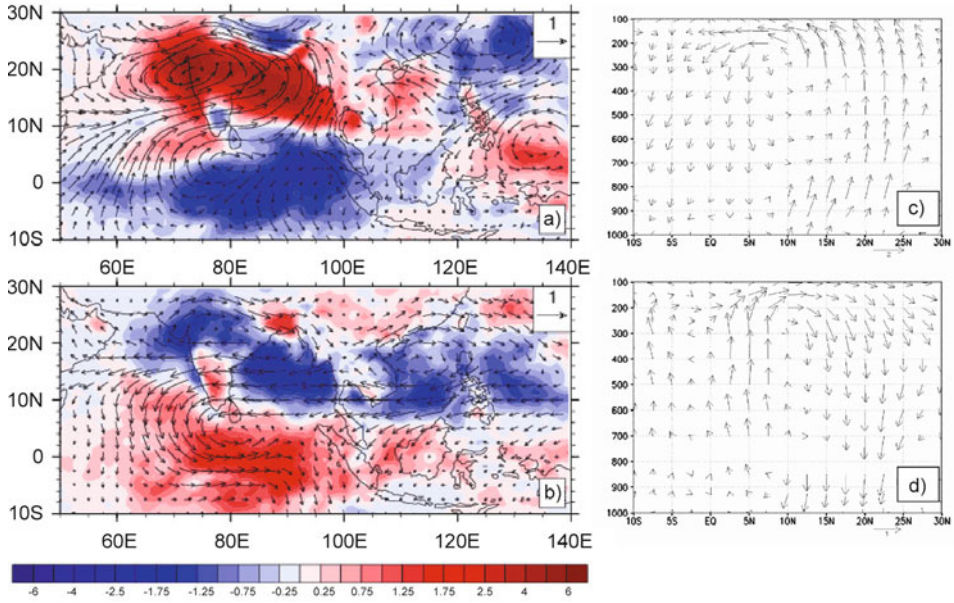

Figure 2.5. Horizontal and vertical structure of dominant ISV. Regressed 10 to 90-day filtered GPCP (shaded, mm day^{-1}) and zonal and meridional wind anomalies at 850 hPa (vectors, m s^{-1}) with respect to the ISO index (Figure 2.4) at (a) 0 lag (active condition) and (b) 14-day lag (break condition). (c) and (d) The anomalous regional Hadley circulation associated with active and break conditions, respectively. Regressed meridional and vertical wind anomalies at a number of vertical levels averaged over 75°E–85°E. Vertical wind anomalies (h Pa s^{-1}) have been scaled up by a factor of 100.

circulation is significantly strengthened (weakened) during the active (break) phase. The anomalous Hadley circulation also indicates a baroclinic vertical structure for monsoon ISV.

Within the broad range of 10 to 90-day periods, two period ranges, with periodicities between 10 and 20 days and 30 and 60 days, respectively, are particularly prominent. Several early studies (Murakami, 1976; Krishnamurti and Bhalme, 1976) showed the existence of a 10 to 20-day oscillation in a number of monsoon parameters. Later studies (Krishnamurti and Ardunay, 1980; Chen and Chen, 1993) show that the 10 to 20-day oscillation is a westward-propagating mode closely related to monsoon active/break conditions. In addition to the 10 to 20-day oscillation, a prominent oscillation with a 30 to 60-day period is seen in monsoon circulation (Dakshinamurthy and Keshavamurthy, 1976), cloudiness, and precipitation (Yasunari, 1979, 1980, 1981; Sikka and Gadgil, 1980). Most of these early studies estimated the spectral peaks based on limited data and, hence, it was not possible to establish the statistical significance of the peaks. The existence of significant power in the two frequency ranges is illustrated in Figure 2.6 where the power spectra of four representative time series are shown. One (Figure 2.6a) is of

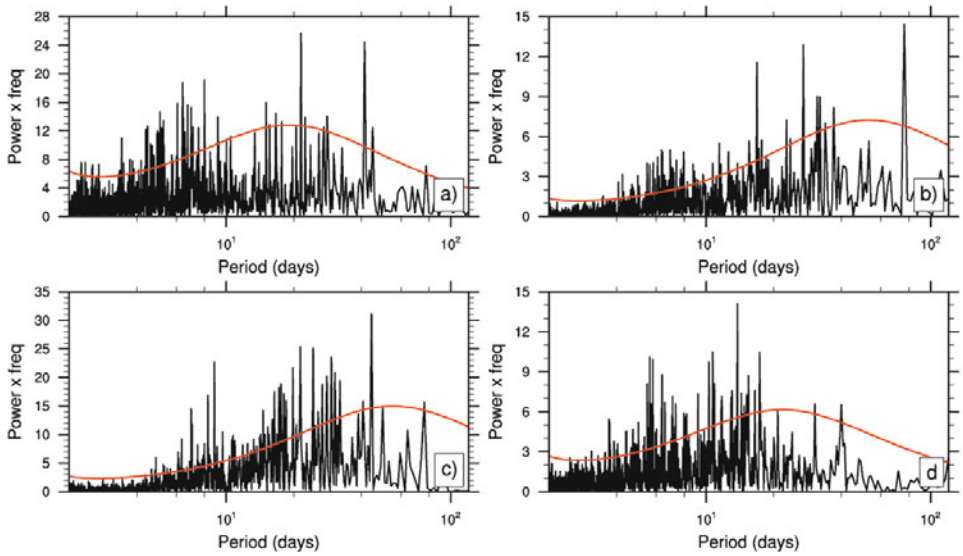

Figure 2.6. Spectrum of (a) rainfall anomalies for 20 (1979–1998) summer seasons (June 1–September 30) from IMD high-resolution gridded rainfall data averaged over 75.5°E–85.5°E and 15.5°N—25.5°N, and (b) zonal wind anomalies at 850 hPa for 20 (1979–1998) summer seasons from NCEP reanalysis averaged over 55°E–65°E and 5°N–15°N (Arabian Sea). (c) Same as (b) but averaged over 85°E–90°E and 10°N–15°N (Bay of Bengal). (d) Same as (b) but for meridional wind anomalies averaged over 80°E–85°E and equator–5°N. Spectra are calculated using the periodogram method and the dotted lines represent a 95% confidence level with respect to a red noise null hypothesis.

daily precipitation anomalies from the raingauge data (Rajeevan *et al*., 2006) averaged over 75.5°E–85.5°E and 15.5°N–25.5°N (central India) for 20 (1979–1998) summer seasons (June 1–September 30) while two others (Figure 2.6b, c) are of daily zonal wind anomalies at 850 hPa from NCEP reanalysis averaged over 55°E–65°E and 5°N–15°N (Arabian Sea, or AS) and over 85°E–90°E and 10°N–15°N (BoB) also for 20 summer seasons, respectively. The last one (Figure 2.6d) is of meridional wind anomalies averaged over 80°E–85°E and equator–5°N. A strong quasi-biweekly period is seen in the precipitation time series (Figure 2.6a) distinct from synoptic variability (period <10 days) and the lower frequency 30 to 60-day mode. Significant power at the 10 to 20-day range is also noted in the two zonal wind time series. It is also noted that the zonal winds at low levels over the BoB (Figure 2.6c) have higher power at this frequency range than those over the AS (Figure 2.6b). The meridional wind over the central equatorial IO (Figure 2.6d) shows prominent power at 10 to 20-day timescales well separated from synoptic disturbances and the low-frequency 40-day mode. There is also significant power at the 30 to 60-day ranges in all the four time series.

To put the role of these two oscillations in the context of variability of full daily anomalies, zonal wind anomalies at 850 hPa between June 1 and September 30 for 20

years were bandpass-filtered to retain periods between 10–20 days and 30–60 days using a Lanczos filter. The ratio between variances of the 10 to 20-day modes and of the 30 to 60-day modes and that of total daily anomalies are shown in Figure 2.7. It may be noted that variance of zonal winds at low level contributed by each of these modes is considerable, ranging between 15% and 25% of total daily variance. However, the importance of the two ISO modes go far beyond these percentages of total daily variance explained, as ISOs strongly modulate the synoptic activity (see Section 2.4) responsible for a large fraction of total daily variability. The global structure of the 30 to 60-day oscillation has been explored in a number of studies (Krishnamurti *et al*., 1985; Knutson *et al*., 1986; Lau and Chen, 1986; Murakami *et al*., 1986; Knutson and Weickmann, 1987; Nakazawa, 1986). In contrast, the spatial structure and propagation characteristics of the 10 to 20-day mode has been addressed only by a few studies (Krishnamurti and Ardunay, 1980; Chen and Chen, 1993; Goswami and Ajaya Mohan, 2001; Chatterjee and Goswami, 2004). It may be noted that the 10 to 20-day and 30 to 60-day ISV is not unique to the SA monsoon. The EA/WNP monsoon also exhibits 12 to 24-day and 30 to 60-day variability during boreal summer (see Chapter 3).

The primary features of the horizontal and vertical structures of the two modes are summarized here. The QBW mode (12–24 days) tends to occur regionally and is found to be associated with monsoons. Kikuchi and Wang (2009) identify three

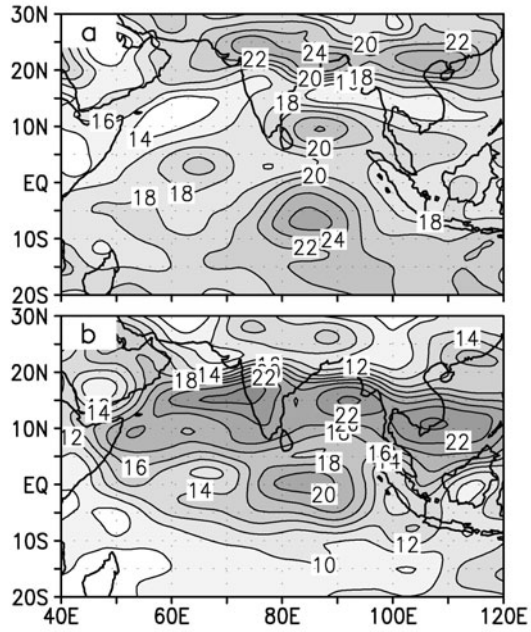

Figure 2.7. Percentage of total daily variance of 850 hPa zonal winds explained by (a) 10 to 20-day mode and (b) 30 to 60-day mode during the summer monsoon season (June 1–September 30) for 20 years (1979–1998).

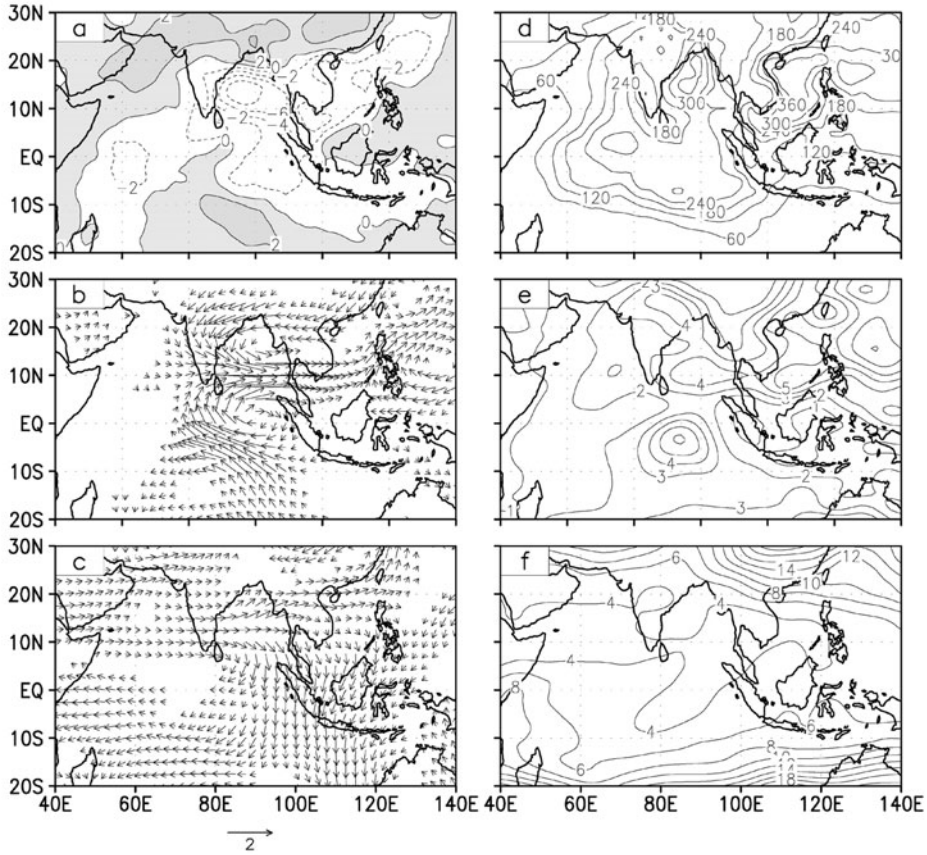

Figure 2.8. Spatial structure and amplitude of the 10 to 20-day mode. Regressed 10 to 20-day filtered anomalies of (a) OLR (in $W\,m^{-2}$), (b) 850 hPa winds, and (c) 200 hPa winds (in $m\,s^{-1}$) with respect to a reference time series of 10 to 20-day filtered zonal winds averaged over 85°E–90°E and 5°N–10°N with 0 lag. Only regressed wind anomalies significant at 95% confidence level are plotted, with a mean variance of 10 to 20-day filtered (d) OLR (in $W^2\,m^{-4}$), (e) 850 hPa, and (f) 200 hPa zonal winds (in $m^2\,s^{-2}$) based on 20 (1979–1998) summers (June 1–September 30).

boreal summer QBW modes in the Asia–Pacific, Central America, and subtropical South Pacific regions. They also find five austral summer QBW modes in the Australia–southwest Pacific, South Africa–Indian Ocean, South America–Atlantic, subtropical North Pacific, and North Atlantic–North Africa regions. The horizontal and vertical structure of the 10 to 20-day mode is illustrated in Figure 2.8. A reference time series is constructed by averaging 10 to 20-day filtered zonal winds at 850 hPa over a box between 85°E–90°E and 5°N–10°N during the summer season (June 1—September 30) for 20 years (1979–1998). The reference box is selected to be in a region of high variance of 10 to 20-day filtered zonal winds at 850 hPa. Lag

regressions with the reference time series of 10 to 20-day filtered zonal and meridional winds at 850 hPa and 200 hPa, together with that of outgoing longwave radiation (OLR) at all gridpoints, are constructed. Simultaneous regressed OLR and wind vector anomalies at 850 hPa and 200 hPa are shown in Figure 2.8a, b, c, respectively. The low-level wind structure of the mode is characterized by two vortices: one centered around 18°N while the other has its center close to the equator around 3°S. It may be recalled that the gravest meridional mode ($n = 1$) equatorial Rossby wave is also characterized by two vortices similar to those in Figure 2.8b, but centered around the equator (Matsuno, 1966; Gill, 1982). It has recently been shown (Chatterjee and Goswami, 2004) that the low-level spatial structure of the mode may be interpreted as the gravest meridional mode ($n = 1$) equatorial Rossby wave with a wavelength of about 6,000 km but shifted to the north by about 5° by the background summer mean flow. The phase of the vortices in the vertical remain the same from the surface up to 200 hPa and change sign around 150 hPa, indicating its vertical structure to have a significant barotropic component (see also Chen and Chen, 1993) together with a baroclinic component. The figure also contains average variance associated with 10 to 20-day filtered OLR zonal winds at 850 hPa and 200 hPa (Figure 2.8d, e, f). Significant fluctuations of OLR (standard deviation of 15–20 $W\,m^{-2}$) and zonal winds at both lower and upper levels (2 $m\,s^{-1}$) are associated with this oscillation. Coherent evolution of the OLR and the circulation anomalies throughout the oscillation indicate that convective coupling is involved with the genesis and propagation of the mode. This is further illustrated in Figure 2.9 where regressed OLR and divergence at 925 hPa averaged over 5°N–15°N are shown as a function of

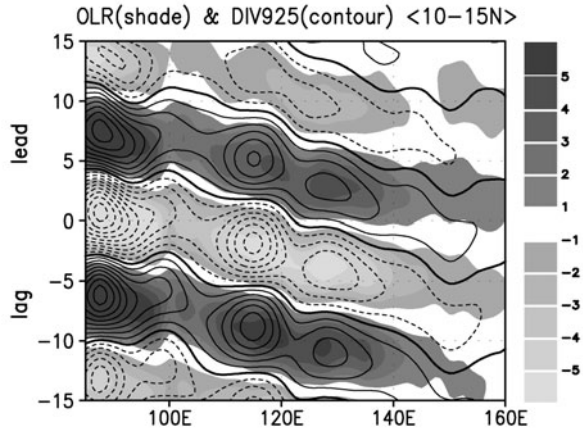

Figure 2.9. Coupling between convection and low-level winds for the 10 to 20-day mode. Lag–longitude plot of regressed 10 to 20-day filtered anomalies of OLR (in $W\,m^{-2}$; shaded) and divergence of 925 hPa winds (contour) with respect to the same reference time series described in Figure 2.8 averaged over 10°N–15°N. Solid (dashed) lines indicate positive (negative) divergence, with a contour interval of $0.1 \times 10^{-6}\ s^{-1}$, and with thick lines showing the zero contour.

longitudes and lags. The close association between boundary layer convergence (divergence) and negative (positive) OLR anomalies is apparent. Also the convergence center being slightly west of the OLR center seems to be responsible for the westward propagation of the mode.

The horizontal structure of the 30 to 60-day mode is studied in a similar manner by constructing a reference time series of 30 to 60-day filtered zonal winds at 850 hPa averaged over 80°E–90°E and 10°N–15°N and calculating lag regressions of 30 to 60-day filtered zonal and meridional winds and OLR everywhere. The simultaneous OLR and vector wind anomalies at 850 hPa and 200 hPa associated with the mode are shown in Figure 2.10a, b, c, respectively. The mean variance associated with the

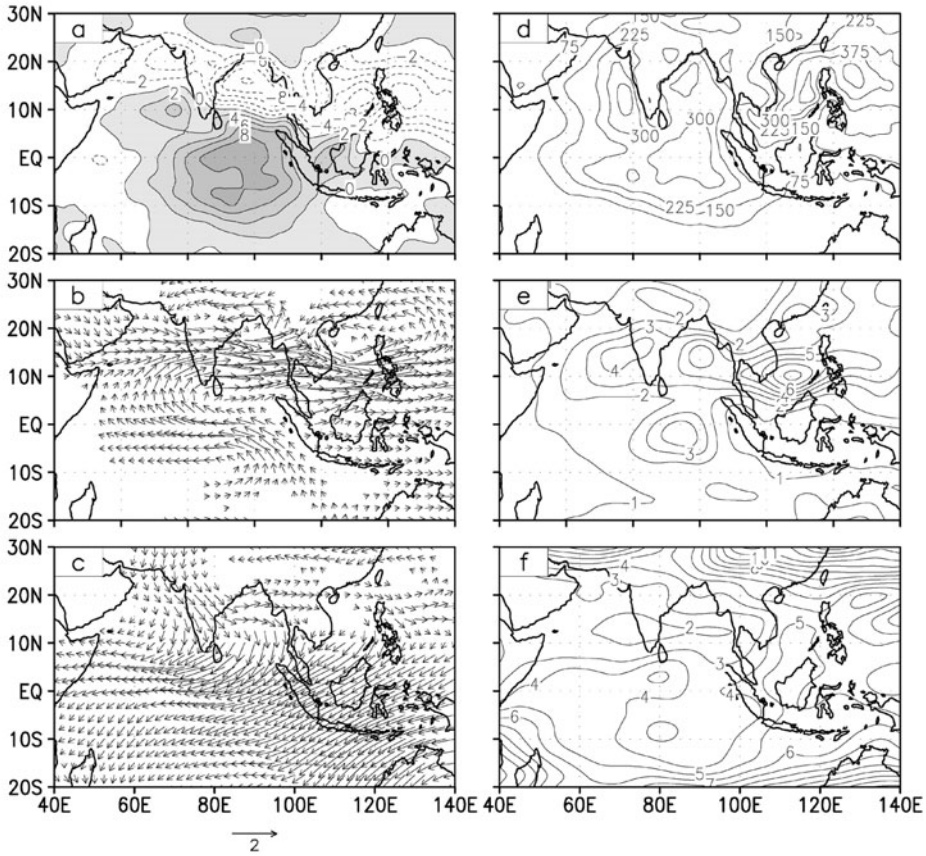

Figure 2.10. Spatial structure and amplitude of the 30 to 60-day mode. Regressed 30 to 60-day filtered anomalies of (a) OLR (in $W\,m^{-2}$), (b) 850 hPa winds, and (c) 200 hPa winds (in $m\,s^{-1}$) with respect to a reference time series of 30 to 60-day filtered zonal winds averaged over 85°E–90°E and 5°N–10°N with 0 lag. Only regressed wind anomalies significant at 95% confidence level are plotted, with a mean variance of 30 to 60-day filtered (d) OLR (in $W^2\,m^{-4}$), (e) 850 hPa, and (f) 200 hPa zonal winds (in $m^2\,s^{-2}$), based on 20 (1979–1998) summers (June 1–September 30).

30 to 60-day filtered OLR and zonal winds at 850 hPa and 200 hPa are shown in Figure 2.10d, e, f, respectively. The spatial structure of OLR and low-level winds associated with the mode are similar to those found in various studies (e.g., Annamalai and Slingo, 2001; Goswami and Ajayamohan, 2001; Webster *et al.*, 1998). The horizontal scale of the 30 to 60-day mode (half-wavelength of about 10,000 km) is much larger than that of the 10 to 20-day mode (Figure 2.8) which is rather regional in character. The other interesting point to note is that the low-level wind anomaly associated with the 30 to 60-day mode (Figure 2.10b) has a structure similar to that of the seasonal mean (Figure 2.10d), strengthening (weakening) the seasonal mean in its active (break) phases. It may also be noted that the horizontal structure of the 30 to 60-day mode around the Indian longitudes is characterized by two vortices of opposite sign flanked on either side of a vortex centered close to the equator, similar to the spatial structure of $n = 2$ equatorial Rossby mode. The difference between the two (e.g., asymmetry in the strength of the northern and the southern vortices and a shift of the vortices to the north) is likely to be due to the modification of the Rossby wave by the summer mean background flow. Comparison of Figure 2.5 and Figure 2.10 indicates that the large-scale structure of active/break conditions seems to come largely from the 30 to 60-day modes. The 200 hPa anomalies associated with the 30 to 60-day mode are opposite to those at low levels but with a tilt to the west. Phase transition takes place (not shown) at around 500 hPa. Therefore, a first baroclinic mode vertical structure emerges for the mode.

In order to gain insight into the spatiotemporal scales associated with boreal summer ISV, spacetime spectra of GPCP rainfall and 850 hPa zonal winds in the east–west direction between 10°S and 25°N are calculated using the procedure followed by Wheeler and Kiladis (1999). The dominant power in both precipitation and low-level winds (Figure 2.11a, b) indicate that the dominant mode with period between 30 and 60 days is eastward propagating with a zonal scale between wavenumbers 1 and 3 and is strongly convectively coupled. To examine the northward propagation characteristics, the spacetime spectra of GPCP rainfall and 850 hPa zonal winds in the north–south direction were also carried out by taking the data between 20°S and 35°N and averaging the spectra between 60°E and 110°E. The dominant mode with period between 30 and 60 days has a strong northward propagation with northward-propagating power between wavenumbers 1 and 3 being nearly four times larger than southward-propagating power of the same wavenumber and frequency band. The strong convectively coupled nature of monsoon ISOs is also demonstrated by Chattopadhyay *et al.* (2008) who show that different nonlinear phases of rainfall ISO can be uniquely identified by a set of dynamical parameters, without explicitly involving rainfall itself.

Coherent evolution of OLR and relative vorticity anomalies at 850 hPa shown in Figure 2.12 over a cycle of the oscillation indicate strong convective coupling for the 30 to 60-day mode also. The evolution of OLR anomalies over a cycle of the 30 to 60-day mode is similar to that found in other studies (e.g., Annamalai and Slingo, 2001) using other methods. One interesting point that emerges from this figure is that

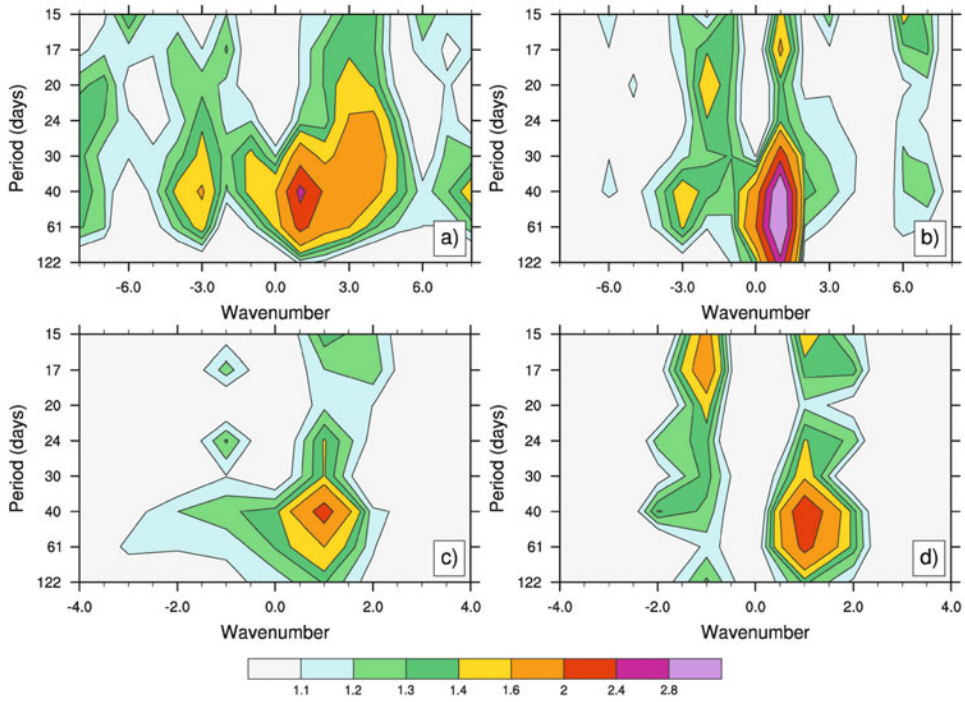

Figure 2.11. Th top panel shows symmetric east–west wavenumber–frequency spectra normalized by its red background calculated for 11 JJAS seasons for the 1997–2007 period calculated using (a) precipitation (GPCP) and (b) U850 anomalies. The bottom panel shows north–south wavenumber–frequency spectra normalized by its red background calculated for 11 JJAS seasons for the 1997–2007 period (60°E–100°E,12.5°S–29.5°N) calculated using (c) precipitation (GPCP) and (d) U850 anomalies.

the 30 to 60-day variability over the SA monsoon region and that over the EA/WNP region (see Chapter 3) during boreal summer is governed by the same 30 to 60-day mode of variability. The main difference being that the phase of northward propagation of the mode in the EA/WNP is shifted with respect to that over the SA monsoon region by about 10 days. The convection first starts in the equatorial IO (day −20) and moves northward to about 10°N (day −10) when convection starts in the south China Sea region. When the convection reaches 25°N in the SA region by day 0, it progresses to about 15°N in the EA/WNP region. Another important point to note is that bands of cyclonic (anticyclonic) relative vorticity at 850 hPa move coherently northward with bands of negative (positive) OLR anomalies with relative vorticity maxima being about 3°N of convection maxima. We shall show later (see Section 2.2.1.1) that this phase relationship between convection and low-level relative vorticity is important for understanding the mechanism of northward propagation of the mode.

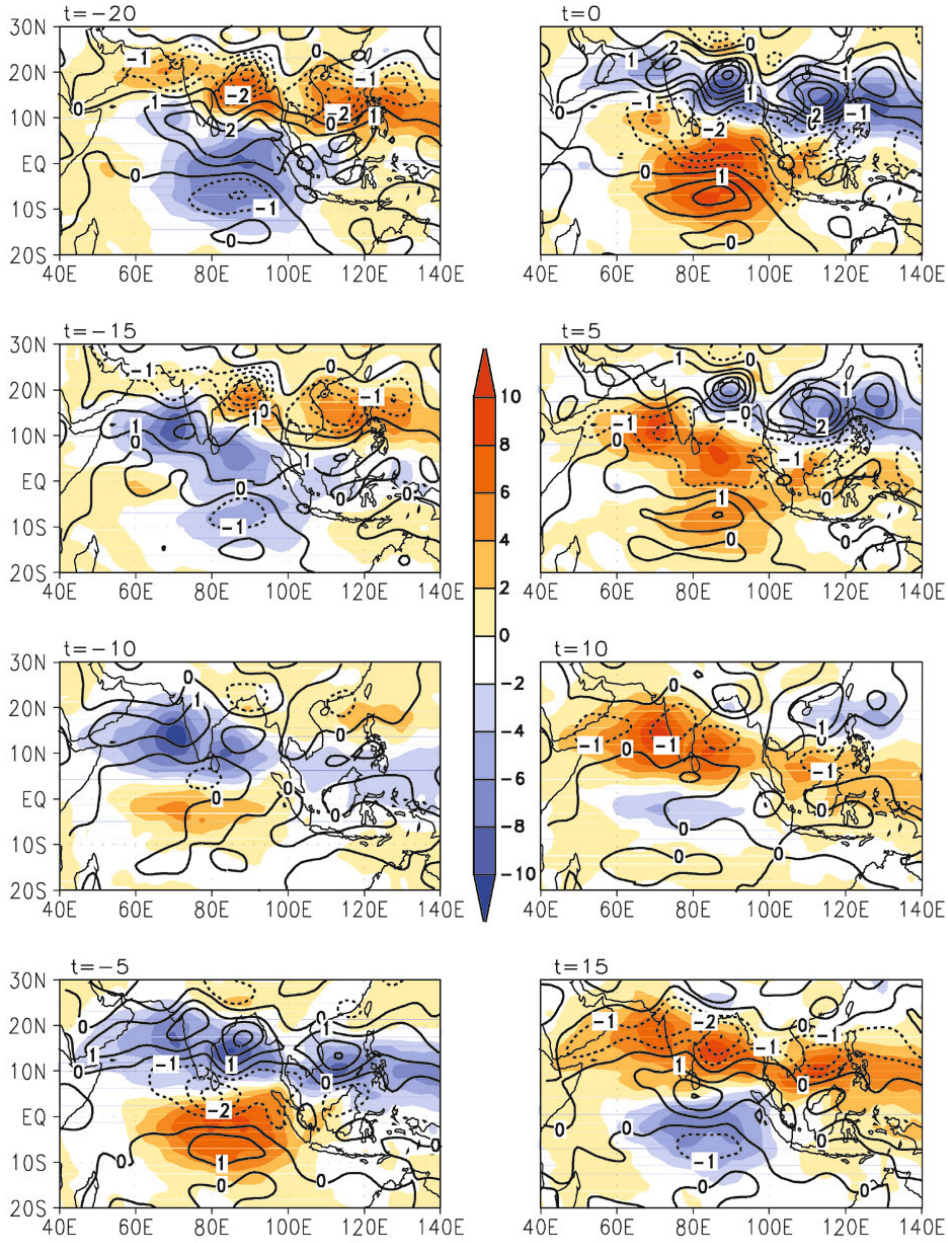

Figure 2.12. Evolution of convection and relative vorticity at 850 hPa over a cycle of the 30 to 60-day mode. Regressed 30 to 60-day filtered anomalies of OLR (in $\mathrm{W\,m^{-2}}$; shaded) and relative vorticity of 850 hPa winds (contour) with respect to the same reference time series described in Figure 2.10 from a lag of 20 days ($t = -20$) to a lead of 15 days ($t = 15$). Solid (dashed) lines indicate positive (negative) relative vorticity, with a contour interval of $1 \times 10^{-6}\ \mathrm{s^{-1}}$, and with thick lines showing the zero contour.

2.1.3 Regional propagation characteristics

The seminal work of Yasunari (1979) and Sikka and Gadgil (1980) led to the discovery that the zonally oriented cloud band of the Tropical Convergence Zone (TCZ) repeatedly propagates northward starting from south of the equator to the foothills of the Himalayas during the summer monsoon season and that the propagation of this cloud band is intimately associated with the active and break cycles of monsoon ISV (Krishnamurti and Subrahmanyam, 1982; Murakami *et al.*, 1984; Webster *et al.*, 1998). In terms of the two modes, northward propagation is primarily associated with the 30 to 60-day mode. Regressed anomalies of relative vorticity based on 30 to 60-day filtered data for 20 summer seasons averaged over 80°E–90°E (Figure 2.13a) illustrate that, on the average, the mode propagates northward north of the equator up to about 25°N and southward south of the equator to about 10°S (not shown). The phase speed of northward propagation is about 1° latitude per day. Similar regressed anomalies averaged between 10°N and 20°N as a function of longitude and lag (Figure 2.13b) indicate a rapid eastward phase propagation at a rate of about $10\,m\,s^{-1}$ for the mode at this latitude belt between 40°E and 80°E and almost stationary in character between 80°E and 140°E. Although the northward propagation characteristics of the mode over Indian longitudes is rather robust, there is considerable event-to-event and year-to-year variability (not shown). In some years (e.g., 1979) there were several

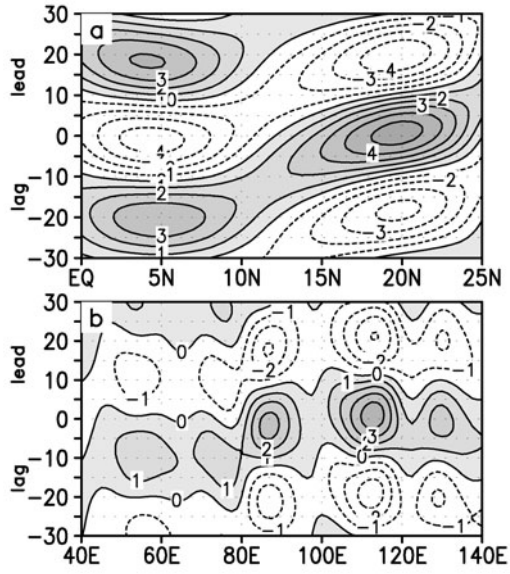

Figure 2.13. (a) Lag–latitude section of regressed anomalies of 30 to 60-day filtered 850 hPa relative vorticity ($10^{-6}\,s^{-1}$) with respect to the same reference time series described in Figure 2.10 and averaged over 80°E–90°E. (b) Lag–longitude section of regressed anomalies of 30 to 60-day filtered 850 hPa relative vorticity ($10^{-6}\,s^{-1}$) with respect to the same reference time series described in Figure 2.10 and averaged over 10°N–20°N.

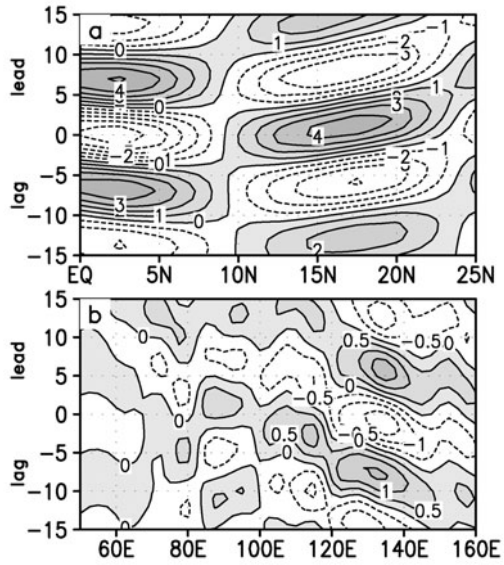

Figure 2.14. (a) Same as Figure 2.12(a), but for the 10 to 20-day mode. (b) Same as Figure 2.13(b), but for the 10 to 20-day mode of regressed anomalies averaged over 5°N–15°N. The reference time series used is the same as that described in Figure 2.8.

regular northward-propagating periods extending up to 25°N while in some other years (e.g., 1981), the northward-propagating periods seem to be terminated at about 15°N. In yet other years (e.g., 1986) there were very few clear northward-propagating periods. While the averaged northward propagation (Figure 2.13a) is a measure of regularity and predictability, it coexists with a certain amount of irregularity that limits the predictability of the mode.

A plot similar to Figure 2.12a for the 10 to 20-day mode (Figure 2.14a) shows that this mode is not associated with any significant northward propagation (Krishnamurti and Ardunay, 1980; Yasunari, 1981; Chen and Chen, 1993). However, the mode is clearly associated with westward propagation from the western Pacific to about 70°E (Figure 2.14b). Both Figure 2.9 and Figure 2.14b indicate that the phase speed of westward propagation is about 4.5 m s^{-1} (Krishnamurti and Ardunay, 1980; Chen and Chen, 1993; Chatterjee and Goswami, 2004). Another point to note from Figure 2.9 and Figure 2.14b is that the 10 to 20-day mode over the SA monsoon region is closely linked with that over the EA/WNP monsoon region during northern summer and that westward propagation from the EA/WNP monsoon region influences the 10 to 20-day variability over the SA monsoon region (Fukutomi and Yasunari, 1999; Annamalai and Slingo, 2001).

2.1.4 Relationship between poleward-propagating ISOs and monsoon onset

SA summer monsoon ISOs are strongly tied up with the annual evolution of the mean monsoon. A notable event in the seasonal evolution of the Indian summer

monsoon is the onset, representing a sudden transition from dry to wet conditions of the annual cycle. Although no objective criterion exists for fixing the date of onset of the SA monsoon, the primary indicator from early days of Indian meteorology has been a sharp and sustained increase in rainfall at a group of stations in Kerala in the southern tip of the Indian continent (Ananthakrishnan *et al*., 1967). Dramatic changes in some of the regional circulation features are known to occur around the time of the onset (Pearce and Mohanty, 1984; Krishnamurti, 1985; Ananthakrishnan and Soman, 1988a, b; Soman and Krishna Kumar, 1993; Joseph *et al*., 1994). A dramatic feature of the onset is the sudden increase in precipitation over the monsoon region (70°E–110°E, 10°N–30°N) followed by a sudden increase of the kinetic energy (KE) over the low-level jet (LLJ) region (55°E–65°E, 5°N–15°N) by a factor of 5 to 10. This is illustrated in Figure 2.15 where the northward propagation of precipitation anomalies (from CMAP) averaged over 70°E–90°E together with the KE of winds at 850 hPa averaged over 55°E–65°E and 5°N–15°N for 3 years are shown. Almost invariably, onset of the monsoon is triggered by a poleward-propagating monsoon ISOs. It may also be noted that a northward-propagating ISO pulse in April or early May does not lead to onset. A northward-propagating pulse of convection and precipitation in early May, as in 1979 (also in 1995 and 2002) is often called a bogus onset (Flatau *et al*., 2001, 2003) and sometimes could be confused as the real onset. The bogus onset is usually associated with a bifurcation of the Madden–Julian Oscillation (MJO) over the BoB. While the dynamic and thermodynamic conditions over the Indian region are not yet ready for the onset, they lead several days later to onset of the East Asian or south China Sea monsoon (Lau *et al*., 2002) (see also Chapter 3). Real onset is substantially delayed during years with a bogus onset. Delayed onset (as in 1979) or early onset (as in 1984), therefore, depend on the phase of the first pulse of the northward-propagating monsoon ISOs. The interannual variability of the phase of the first monsoon ISO and, hence, that of the onset seems to be related to, among others, sea surface temperatures (SSTs) over the south tropical IO and western equatorial Pacific (Joseph *et al*., 1994; Flatau *et al*., 2003).

While the high level of mean KE of the LLJ is maintained by the large-scale non-adiabatic tropospheric heat source that is set up by Tibetan Plateau heating and deep convection over India and the BoB (Li and Yanai, 1996), the fluctuations of total KE of the LLJ within the season are closely related with the intraseasonal fluctuations of precipitation (non-adiabatic heating) over India and BoB. The northward-propagating pulse of precipitation ISOs over India and the BoB in September, however, does not accelerate the LLJ over the AS. This may be understood if we keep in mind that the wind response depends on the spatial structure of the non-adiabatic heat source. The center of non-adiabatic heating moves eastward with the season and is centered around 10°N and 100°E in September due to a decrease of sensible heating over the Tibetan Plateau (Yanai and Tomita, 1998). As a result, the cross-equatorial flow shifts to the central and eastern IO during September and is not reflected in the KE of western IO winds.

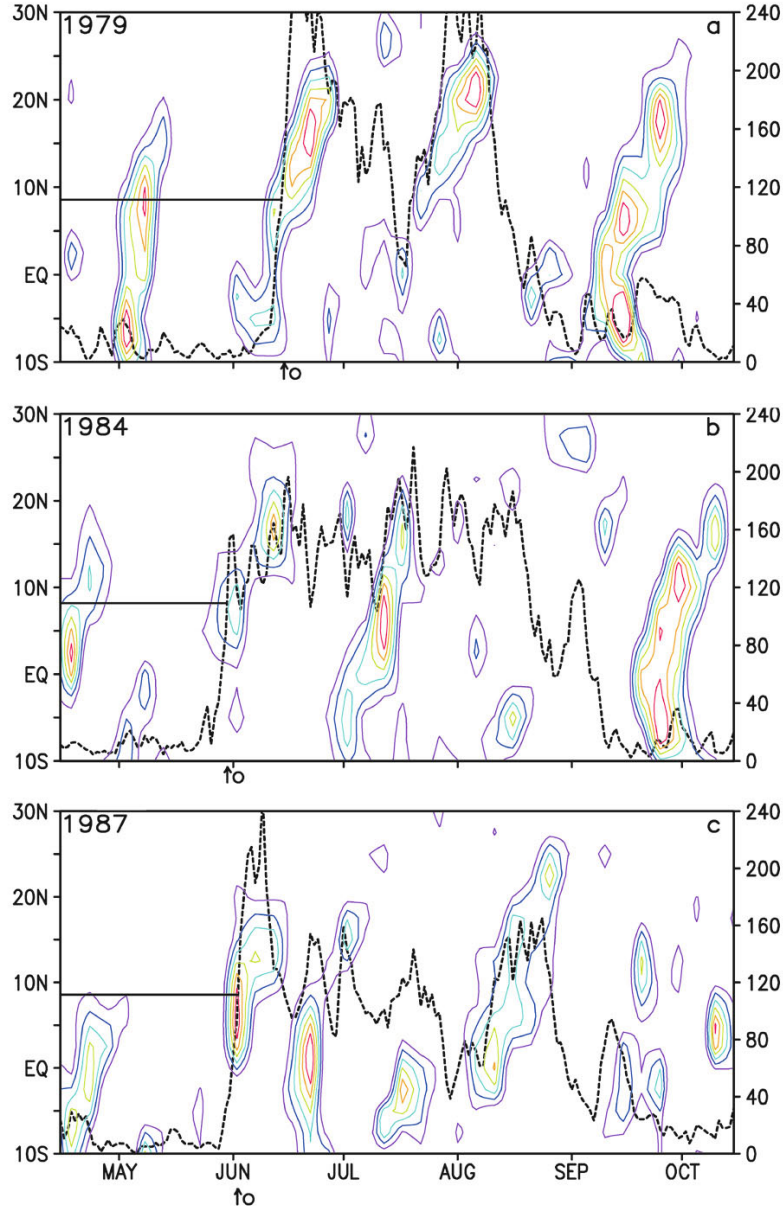

Figure 2.15. Time–latitude section of CMAP anomalies (unfiltered) averaged over 70°E–90°E. Only positive anomalies greater than 2 mm day^{-1} with a contour interval of 2 mm day^{-1} are plotted. Northward-propagating wet spells can be seen. The dashed line shows the evolution of total KE of winds at 85O hPa averaged over the LLJ (55°E–65°E, 5°N–l5°N). The scale for the KE (m s^{-1})^2 is on the right. The latitude of Kerala (southern tip of India) is shown by the horizontal line. The monsoon onset over Kerala is shown by the arrow and roughly corresponds to KE exceeding 100(m s^{-1})^2 and precipitation exceeding 4 mm day^{-1}.

2.1.5 Relationship with the MJO

An oscillation with a period between 30 and 60 days confined around the equator, generally known as the MJO, was discovered in the early 1970s and has since been studied extensively (see Chapters 1 and 7–12 for details). The MJO is strongest during the boreal winter and spring seasons when it appears as an eastward-propagating large-scale system in convection, zonal winds, and upper-level velocity potential (Hendon and Salby, 1994). During boreal summer, while the MJO is typically weaker and more complex in character (Madden, 1986; Madden and Julian, 1994), the northward-propagating monsoon ISO is vigorous. The similarity in temporal character of the two ISOs raises a natural question: Are the two in any way related? This question led some authors (Yasunari, 1979; Lau and Chen, 1986; Madden and Julian, 1994) to suggest that the northward-propagating convection over the Indian monsoon region is related to eastward-propagating clouds along the equator. Tracing all the 122 intraseasonal systems in pentad mean intraseasonal OLR (equivalent to 10 to 90-day filtered) data between 1975 and 1985, Wang and Rui (1990) conclude that almost half of the northward-propagating events during boreal summer were not associated with eastward-propagating equatorial convection (MJOs). Building on the study of Wang and Rui (1990), a comprehensive study based on 24 years of convection data was carried out by Jones *et al.* (2004) using more objective tracking of convection anomalies. They arrived at conclusions similar to those of Wang and Rui (1990) for the summer ISOs. With the higher sample size compared with that of Wang and Rui (1990), they could also study some IAVs of summer ISOs. Using an index of ISV based on the first two empirical orthogonal functions (EOFs) of 25 to 80-day filtered OLR anomalies between 1975 and 1999 (excluding 1978), Lawrence and Webster (2001) conclude that about 78% of northward-moving convection is associated with eastward-moving convection at the equator, although they also found some independent northward-moving events. The discrepancy between their study and that of Wang and Rui (1990) on the fraction of independent northward-propagating events appear to be partly due to the fact that only a small fraction (about 20%) of the total ISO variance is represented by the ISO index of Lawrence and Webster (2001), and partly due to a different criterion being used in the latter study to define independent northward-moving events. While a fraction of boreal summer events are associated with an eastward-propagating MJO, a significant fraction (up to 50%) of them are independent northward-moving events. The northward-propagating character, larger meridional scale, and weaker eastward penetration make summer ISOs distinct from the winter MJO (Jones *et al.*, 2004). As a result, MJO theories may not be sufficient to explain the genesis or northward movement of the full spectrum of summer monsoon ISOs.

Pai *et al.* (2009) examine the association of different phases of the MJO as defined by Wheeler and Hendon (2004) MJO indices (RMM1 and RMM2) with active and break phases of the monsoon over India. While no strong signal has emerged, they find that the initiation as well as the duration of the break phases seem to occur with MJO phases 7, 8, 1, and 2. They also find that possibility for

onset of active events was relatively higher during phases 3 to 6. A new linkage between an eastward-propagating MJO and a northward-propagating summer ISO has come to light recently (Joseph *et al*. 2009), though there is considerable interannual variation of MJO power (with a period between 30 and 60 days and an eastward wavenumber between 1 and 3) during boreal summer. While MJO power is strong during winter and weak during summer, in the summer of Indian monsoon drought years it is found to be as strong as during winter. On the other hand, during the summer of Indian monsoon flood years, eastward-propagating power is even weaker than westward-propagating power (fig. 6 of Joseph *et al*. 2009). During drought years, the MJO triggers an air–sea interaction, leads to a ''long break'', and plays a crucial role in creating the drought.

2.2 MECHANISM FOR TEMPORAL-SCALE SELECTION AND PROPAGATION

As noted in Figure 2.7, both ISOs are significant, each explaining 15% to 25% of daily variability. Although they are not single-frequency sinusoidal oscillations, peak power around the broadband spectrum indicates preferential excitation and amplification around these frequencies. A question naturally arises: What is responsible for the preferential excitation and amplification around these frequencies? Such a mechanism must also explain the very large horizontal scale and northward movement of the 30 to 60-day mode and smaller horizontal scale and westward propagation of the 10 to 20-day mode. We also noted that evolution of circulation is strongly coupled with that of convection and precipitation for both modes. The interaction between organized convection and flow (circulation) must, therefore, be at the heart of explaining not only the basic preferred periodicities but also their propagation characteristics.

2.2.1 30 to 60-day mode

The seasonal mean summer monsoon is characterized by two maxima in rainfall: one over the monsoon trough region between 15°N and 25°N and another in the IO between the equator and 10°S. Both locations are associated with low-level cyclonic vorticity and represent two preferred locations of the TCZ. The oceanic preferred location is associated with an SST maximum (Hastenrath and Lamb, 1979) in the region, and the oceanic TCZ is maintained by the meridional gradient of SST and zonally symmetric dynamics discussed in several studies (Schneider and Lindzen, 1977; Held and Hou, 1980; Goswami *et al*., 1984). The off-equatorial location is along the monsoon trough (MT), a low-level quasi-stationary cyclonic vorticity arising from the interaction of cross-equatorial flow and the Himalayan topography. Cross-equatorial flow is set up by a large-scale pressure gradient due to the large-scale non-adiabatic heating gradient. Tomas and Webster (1997) study the role of inertial instability in maintaining such off-equatorial precipitation when the zero potential vorticity line is located off the equator due to the large-scale north–south

surface pressure gradient. Since the horizontal scale of the 30 to 60-day mode is large and similar to that of the seasonal mean (Figure 2.10), the mode appears as fluctuations of the TCZ between the two preferred locations (Sikka and Gadgil, 1980; Krishnamurti and Subrahmanyam, 1982; Goswami, 1994). The dynamics of the zonally symmetric TCZ, therefore, provide a paradigm for understanding the genesis and northward propagation of the 30 to 60-day mode (Webster, 1983; Goswami and Shukla, 1984; Nanjundiah *et al*., 1992; Srinivasan *et al*., 1993). Webster (1983) simulated northward-propagating ISOs in a zonally symmetric model with land north of 14°N and an advective mixed layer ocean south of it (hereafter referred to as the W-model). The simulated ISOs, however, had a period of about 15 days and, unlike observed ISOs, started from the land–ocean boundary. Using a zonally symmetric version of the GLAS (Goddard Laboratory for Atmospheric Sciences) global circulation model (GCM), Goswami and Shukla (1984) simulate the ISO of the TCZ during northern summer as having a period and northward propagation similar to those observed. The simulated unfiltered precipitation band (fig. 4 in Goswami and Shukla, 1984) starts from about 5°S and has a longer residence time over the northern location of the TCZ, similar to the characteristics of the observed cloud band (Sikka and Gadgil, 1980). They further show that the simulated ISO with a period similar to that observed arises due to an interaction between organized convection and large-scale Hadley circulation. According to their convection–thermal relaxation feedback mechanism, convective activity results in an increase of static stability which depresses the convection itself. Meanwhile, dynamic processes and radiative relaxation decrease moist static stability and bring the atmosphere to a new convectively unstable state.

Gadgil and Srinivasan (1990) and Srinivasan *et al*. (1993) derive additional insight regarding factors responsible for determining the period of the oscillations by experimenting with the W-model. They show that poor simulation of the period of the ISO by the original W-model was due to the model not taking the thermal inertia of land and low moisture holding capacity into consideration. With the W-model modified to include the increased thermal inertia of the land and increased moisture holding capacity (from 10 cm to 30 cm), Srinivasan *et al*. (1993) are able to simulate the observed periodicity of ISOs. The zonally symmetric mixed layer in the W-model had a large cold bias in simulating the meridional structure of SST over the IO region. The prescription of observed SST avoided this bias and allowed simulation of northward propagation of the oscillations from near the equator.

The very large zonal scale compared with the meridional scale of the dominant summer monsoon ISO invited zonally symmetric dynamics to be invoked as an explanation of the genesis and temporal-scale selection. However, these theories do not shed light on the observed zonal phase propagation of a large fraction of the summer ISOs. Therefore, wave dynamics needs to be involved for a fuller explanation of the genesis and phase propagation of ISOs. Krishnan *et al*. (2000) indicate that westward-propagating Rossby waves are important in causing the transition from an active to a break phase of summer ISOs. As the theory for

genesis and eastward-propagating MJO is much better developed (see Chapter 10) in terms of an equatorial convectively coupled Kelvin–Rossby couplet, some attempts have been made (Lau and Peng, 1990; Wang and Xie, 1997) to seek an explanation for scale selection and northward propagation of summer monsoon ISOs within the same framework. Lau and Peng (1990) show that the interaction of eastward-propagating equatorial ISOs with mean monsoon flow can lead to an unstable quasi-geostrophic baroclinic Rossby wave with a wavelength of 3,000 km to 4,000 km over the Indian monsoon region between 15°N and 20°N. As these waves grow, low-level air is drawn northward resulting in rapid northward propagation of the area of deep convection. Based on the results of a modeling study, Wang and Xie (1997) describe summer ISOs as a convection front formed by continuous emanation of equatorial Rossby waves from convection in the equatorial western Pacific. An initial convection cell over the equatorial IO moves eastward as a Kelvin wave and forms Rossby wave cells on either side with a typical scale of 2,000 km to 4,000 km. Feedback from convection and westward propagation of emanated Rossby waves makes the convection front tilt northwestward from the equator to 20°N, resulting in an apparent northward movement. The westward-propagating Rossby waves eventually decay over the AS due to a dry airmass from Africa sinking while a southern cell initiates equatorial perturbation and starts the next cycle. The lifecycle takes about 4 weeks.

Thus, convectively coupled wave dynamics involving a Kelvin and Rossby wave pair can give rise to an ISO with a timescale of 30–40 days. This mechanism is probably responsible for summer monsoon ISOs that are associated with eastward propagation at the equator. A significant fraction of summer ISOs have northward-moving events not associated with eastward-moving equatorial disturbances. Zonally symmetric dynamics is required to explain these summer ISOs as wave dynamics cannot explain the genesis of this fraction of summer ISOs. Thus, both wave dynamics and zonally symmetric physics are required to explain the full range of the summer monsoon 30 to 60-day mode.

2.2.1.1 Mechanism for poleward propagation of the 30 to 60-day mode

As described in Section 1.3, a major characteristic of the 30 to 60-day mode is its poleward propagation. Hence, a considerable amount of literature has been devoted to understanding the poleward propagation of this mode. However, temporal-scale selection and northward propagation are intimately related. Therefore, here we describe how different mechanisms for temporal-scale selection, discussed above, address the question of observed northward propagation of the mode. Webster (1983) propose that the northward gradient of sensible heat flux is responsible for the poleward propagation of the cloud band. Goswami and Shukla (1984) also indicate that ground hydrology feedback may be responsible for northward propagation. Later, Gadgil and Srinivasan (1990) and Nanjundiah *et al*. (1992) show that the northward gradient of moist static stability (the poleward side being more unstable than the equatorward side) is responsible for the poleward propagation of the cloud band. The existence of a meridional gradient of near surface background humidity in this region contributes to the meridional gradient of moist

static stability. While these studies followed a zonally symmetric paradigm and identified some processes that are important for northward propagation, a few other studies (Lau and Peng, 1990; Wang and Xie, 1997) attempted to explain the basic genesis and northward propagation resulting from unstable Rossby waves interacting with the background monsoon mean flow. However, the physical mechanism that led to the northward component of Rossby wave propagation was not clearly identified in these studies. Keshavamurthy *et al.* (1986) also indicate that northward propagation may arise from a zonally symmetric component of an eastward-propagating equatorial oscillation interacting with the mean flow over the Asian monsoon region.

To gain some insight regarding the mechanism responsible for the poleward propagation of the cloud band, a diagnostic analysis is presented here. Lag regression of 30 to 60-day filtered OLR, relative vorticity at 850 hPa, and divergence at 925 hPa with respect to the same reference time series used in Figure 2.10 were carried out. A lag–latitude plot of regression of OLR and 850 hPa relative vorticity averaged over 80°E–90°E are shown in Figure 2.16a, while that for 850 hPa relative vorticity and divergence at 925 hPa are shown in Figure 2.16b. It is seen from Figure 2.16a that, at any given time, cyclonic (anticyclonic) vorticity at 850 hPa is to the north of the negative (positive) OLR anomalies representing cloudy (clear) belts. This is consistent with observations made from Figure 2.12. The cyclonic (anticyclonic) vorticity at 850 hPa is associated with convergence (divergence) of moisture in the boundary layer as seen by the in-phase relationship between the two in Figure 2.16b. Atmospheric circulation driven by diabatic

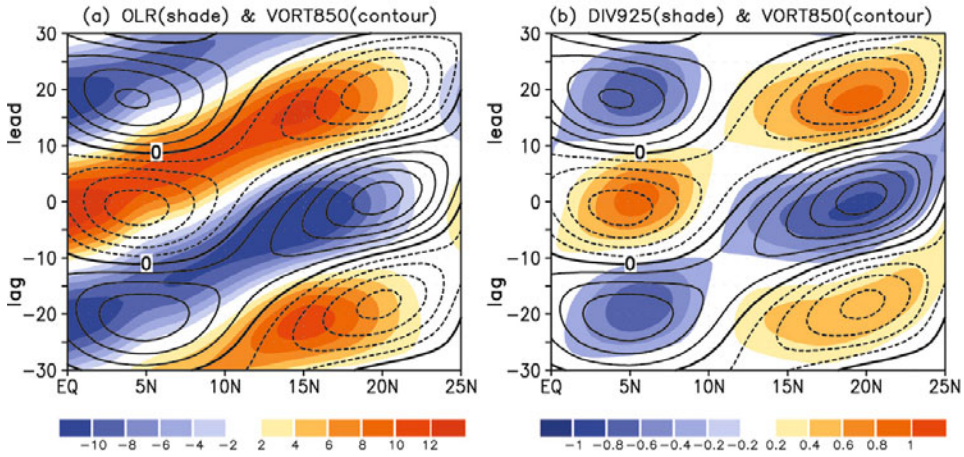

Figure 2.16. (a) Regressed 30 to 60-day filtered anomalies of OLR (shaded; $W\,m^{-2}$) and 850 hPa relative vorticity (contour, positive solid and negative dashed, contour interval $1 \times 10^{-6}\,s^{-1}$) with respect to the reference time series described in Figure 2.10 averaged over 80°E–90°E. (b) Regressed 30 to 60-day filtered anomalies of 850 hPa relative vorticity (contour, positive solid and negative dashed, contour interval $1 \times 10^{-6}\,s^{-1}$) and divergence at 925 hPa (shaded; $10^{-6}\,s^{-1}$) with respect to the same reference time series.

heating (Gill, 1980) associated with the zonally oriented cloud band in the presence of background mean flow with easterly vertical shear produces a cyclonic vorticity with a maximum about 3°N of the center of the cloud band. Cyclonic vorticity drives frictional convergence in the planetary boundary layer and leads to higher moisture convergence north of the cloud band. The meridional gradient of mean boundary layer moisture also helps in making moisture convergence larger to the north of the cloud band. This leads the convection center to move northward. Kemball-Cook and Wang (2001) and Lawrence and Webster (2001) also indicate that the planetary boundary layer convergence maximum, being north of the convection maximum, is responsible for the northward propagation of the summer monsoon 30 to 60-day oscillation. Hsu and Weng (2001) also suggest that a similar frictional convergence driven by low-level vorticity is responsible for the northwestward movement of the EA/WNP monsoon 30 to 60-day oscillations.

The crucial question for northward propagation of the 30 to 60-day mode is to understand what is responsible for producing the low-level vorticity maximum north of the convection maximum. Also, northward propagation takes place from about 5°S, but frictional convergence is ineffective near the equator. Therefore, an alternative mechanism is required to explain northward propagation near the equator. Although several earlier studies (Goswami and Shukla, 1984; Gadgil and Srinivasan, 1990; Nanjundiah *et al.*, 1992), using zonally symmetric dynamics, identified some processes as important for northward propagation of the mode, a clear physical picture had not emerged. Using a simple zonally symmetric model to interpret results from a GCM simulation and observations, Jiang *et al.* (2004) provide a clearer picture of the physical processes responsible for poleward propagation. They proposed that a combination of a vertical windshear mechanism and moisture–convection feedback mechanism is responsible for poleward propagation of the convection band. They showed that easterly mean vertical shear in the region gives rise to the generation of barotropic vorticity to the north of the convection center, which in turn generates barotropic divergence in the free atmosphere north of the convection center. This leads to boundary layer convergence north of the convection maximum. The mean flow and mean boundary layer humidity during the summer monsoon season also allow perturbation moisture convergence to be maximum north of the convection center. Both these processes contribute to poleward propagation of the mode. Near the equator, the moisture–convection feedback mechanism is the dominant mechanism producing poleward propagation. Although this mechanism is essentially based on zonally symmetric dynamics, a similar mechanism may be at work in producing the northward component of the Rossby wave motion in the presence of the background summer mean flow (see Chapter 10).

Bellon and Srinivasan (2006) argue that the f-plane model used by Jiang *et al.* (2004) could not explain scale selection correctly and contended that a linear theory may be sufficient to explain all aspects of northward propagation of BISO. However, Drbohlav and Wang (2005) show that, even in a β-plane model, the northward propagation of BISOs is governed by the mean easterly vertical shear and meridional gradient of low-level mean humidity. The role of these two parameters is further

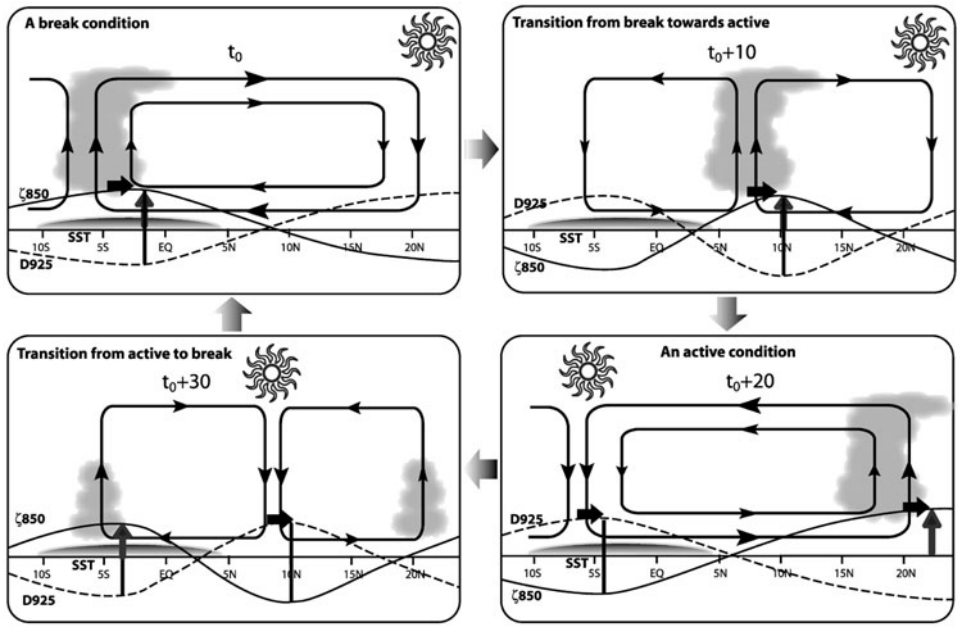

Figure 2.17. A schematic representation of the evolution and northward propagation of the meridional circulation associated with the 30 to 60-day mode in the meridional plane. The thin arrows indicate the anomalous Hadley circulation. The thick vertical arrow indicates the location of the center of boundary layer moisture convergence, while the thick horizontal arrow indicates the direction of poleward motion of the cloud band. The thin solid (dotted) line indicates the phase of relative vorticity at 850 hPa (divergence at 925 hPa) with the positive (negative) phase above (below) the base line. The location of clear sky conditions is shown by the Sun-like symbol.

highlighted by the observation that northward propagation of simulated BISOs in AGCMs and coupled GCMs is strongly linked to the ability of the models to simulate the easterly vertical shear and meridional gradient of low-level humidity (Ajaya Mohan and Goswami, 2007; Ajaya Mohan *et al*. 2010).

Based on understanding the genesis of the large-scale (zonally symmetric) component of the 30 to 60-day mode from modeling studies (e.g., Goswami and Shukla, 1984), and understanding the poleward propagation from diagnostic studies (Figure 2.16) and theoretical analysis (e.g., Jiang *et al*., 2004), the evolution of the mode in the meridional plane over the SA monsoon region is schematically shown in Figure 2.17. The low-level convergence of moisture associated with the SST gradient in a conditionally unstable atmosphere produces organized convection and intensifies the TCZ over the SST maximum over the equatorial IO with subsidence and clear conditions over the MT region (Figure 2.17a). The anomalous Hadley circulation has ascending motion over the oceanic position and descending motion over the MT region. This situation corresponds to a break condition. It is also associated with anomalous cyclonic vorticity over the oceanic location and

anticyclonic vorticity over the MT. Cyclonic vorticity at low levels and the associated boundary layer moisture convergence is maximum north of the zone of maximum convection and makes it move northward (also see Figure 2.16). After about 10 days ($t_0 + 20$, Figure 2.17b) the convection zone reaches about 10°N, with both the MT and oceanic region being under subsidence and clear sky. After another 10 days ($t_0 + 20$, Figure 2.17c), the convection zone reaches the MT zone around 25°N with a divergence maximum slightly north of the anticyclonic vorticity maximum over the oceanic zone (SST maximum). The anomalous Hadley circulation has descending motion over the oceanic position and ascending motion over the MT region. This situation corresponds to an active monsoon condition. During the next 10 days ($t_0 + 30$), the convection over the MT moves farther northward to the foothills of the Himalayas and the clear conditions over the equatorial zone also move northward from 5°S. The decrease in subsidence over the oceanic zone is associated with weak winds, and the continued clear conditions raise the surface temperature as the net heat flux at the surface becomes positive (see also Section 2.3). This acts against subsidence and eventually brings about convection. The convection builds up to become maximum over the oceanic zone in about 10 more days, repeating the cycle.

2.2.2 10 to 20-day mode

In contrast to the considerable attention received by the genesis and scale selection of the summer monsoon 30 to 60-day mode, the 10 to 20-day mode has received very little attention. Having observed that both cloudiness and moist static stability have a quasi-biweekly oscillation, Krishnamurti and Bhalme (1976) propose a mechanism in terms of the cloud–radiation–convection feedback. According to them, the net radiative effect warms up the surface over the MT region under normal summer monsoon conditions and builds up dry and moist static stability of the lower atmosphere. This leads to moist convection, increase in cloud cover, and reduction of solar radiation at the surface. The resultant surface cooling and warming of the middle layer of the atmosphere due to latent heat release associated with the convection stabilizes the temperature profile and cuts down convection. With the dissipation of clouds and increase in solar radiation at the surface, moist instability again builds up and the process can repeat itself. While this is a plausible scenario, Krishnamurti and Bhalme did not demonstrate that the mechanism would preferentially select the quasi-biweekly period. In fact, modeling studies (Goswami and Shukla, 1984; Gadgil and Srinivasan, 1990) indicate that a very similar mechanism leads to the 30 to 60-day oscillation. Chen and Chen (1993) make a comprehensive study of the structure and propagation characteristics of the quasi-biweekly mode (QBM) but did not address the question of scale selection. Using a shallow-water model with a fixed vertical structure and a relaxation timescale for the moisture variable, Goswami and Mathew (1994) propose that the QBM is an unstable mode of the tropical atmosphere driven by the evaporation–wind feedback in the

presence of background westerlies. However, the exact nature of the unstable mode is unclear as the meridional structure is not shown. Also, the zonal wavelength of their most unstable mode is between 9,000 km and 12,000 km, much larger than observed. Chatterjee and Goswami (2004) (hereafter referred to as CG) provide a mechanism for scale selection of the QBM. As shown in Figure 2.8b, c they noted that the horizontal structure of the QBM at low levels resembles that of a first meridional mode ($n = 1$) equatorial Rossby wave with a wavelength of about 6,000 km, but shifted to the north by about 5°. What makes the Rossby wave unstable and affects the selection of observed horizontal scale? A pure $n = 1$ equatorial Rossby wave has two vortices centered around the equator. What is responsible for the northward shift in the structure of the QBM in the meridional direction (Figure 2.8b)? According to CG, the QBM is an equatorial Rossby wave that is driven unstable by convective feedback in the presence of a frictional boundary layer and modified by the summer mean flow.

Using a two-layer atmosphere and a steady Ekman boundary layer with simple parameterization for convective heating, CG showed that convective feedback forced by boundary layer convergence drives an $n = 1$ Rossby wave unstable with maximum growth corresponding to a period of 16 days and a wavelength of 5,800 km. The westward phase speed of the unstable Rossby mode corresponding to this period and wavelength is close to the observed westward phase speed of about 4.5 m s^{-1}. The positive feedback arises from the fact that the baroclinic component of low-level vorticity for the $n = 1$ Rossby wave drives in-phase boundary layer Ekman convergence. As vorticity is in phase with the baroclinic component of potential temperature, latent heat release from boundary layer moisture convergence increases the potential temperature perturbation leading to positive feedback. They noted that turbulent entrainment in the planetary boundary layer is important in achieving the in-phase relationship between convergence in the boundary layer and potential temperature perturbation at the top of the boundary layer. They also demonstrated that inclusion of realistic summertime mean flow in their model results in a shift of the unstable Rossby wave to the north by about 5° without seriously affecting the preferred periodicity and wavelength. The shift of the spatial structure to the north by about 5° can be interpreted as the "dynamic equator" effect. As a free symmetric Rossby wave has the tendency to be centered around background zero absolute vorticity (sum of relative vorticity and Earth's vorticity), the zero background absolute vorticity line may be called the "dynamic equator". The vorticity of background mean flow can make the dynamic equator shift from the geographical equator. It may be noted that low-level summer mean flow makes the zero absolute vorticity line move to about 5°N in the IO/Indonesian region (Tomas and Webster, 1997). The observed shift of the structure of the QBM appears to be due to the shift of the dynamic equator by background mean flow. Thus, this model explains both the scale selection and propagation characteristics of the QBM. It is also shown that the same model may explain the genesis and scale selection of the northern winter QBM observed in the western Pacific.

2.3 AIR–SEA INTERACTIONS

As noted in Section 2.1.2, monsoon ISOs are associated with significant fluctuations of cloudiness and surface winds and, hence, one may expect considerable fluctuations in net heat flux at the surface. What is the amplitude of the net heat flux (Q_{net}) associated with monsoon ISOs? What is the amplitude of intraseasonal SST fluctuations? Do intraseasonal SST fluctuations have a large spatial scale similar to that of atmospheric parameters and Q_{net}? What is the role of SST fluctuations in determining the periodicities and northward movement of monsoon ISOs? We shall attempt to get some answers to these questions in this section.

The first evidence that ISOs involve significant fluctuations of SST and latent heat flux at the interface over the BoB and western Pacific came from Krishnamurti *et al.* (1988) who examined data during 1979 from FGGE (First GARP Global Experiment). While tropical atmosphere and ocean (TAO) moorings in the Pacific have given good data on SST fluctuations associated with the MJO, very little high-resolution direct measurement of SST is available in the IO region. Recent measurements on a few moored buoys by the Department of Ocean Development (DOD) of India (Sengupta and Ravichandran, 2001) have shown large intraseasonal fluctuations of SST and net heat flux over the BoB. Measurements during special field experiments such as BOBMEX (Bhat *et al.*, 2001) and JASMINE (Webster *et al.*, 2002) also show large intraseasonal fluctuations of net heat flux. However, the large-scale structure of ISV of SST was not available, as the IR-based satellite which derived weekly SST (Reynolds and Smith, 1994) was shown to be inadequate to represent observed intraseasonal SST variability (Sengupta and Ravichandran, 2001). With the availability of reliable high-resolution SST measurements using microwave sensors—such as the TMI (TRMM Microwave Imager) on board the TRMM (Tropical Rain Measuring Mission) satellite—it became possible to describe the spatial distribution of ISV of SST over the IO region. Using TMI SST, wind speed, and NOAA OLR data, Sengupta *et al.* (2001) show that an intraseasonal SST oscillation with an amplitude of 0.6°C to 0.8°C has a large horizontal scale similar to that of atmospheric ISOs (Figure 2.5) and possesses northward movement in the region coherent with OLR, surface wind speed, and Q_{net} during the 1998, 1999, and 2000 summer monsoon seasons. Such coherent evolution of 10 to 90-day filtered anomalies of Q_{net}, surface wind speed, precipitation, and SST for the summer season of 2002 is shown in Figure 2.18. The components of net heat flux are estimated using the same formulation used in Sengupta *et al.* (2001). It is noteworthy that the amplitude of interseasonal Q_{net} fluctuations is quite large (70–90 $W\,m^{-2}$). The phase lag between SST and precipitation bands (Figure 2.18, lower panels) is another important aspect of observed summer monsoon ISOs. The warm (cold) SST band follows the dry (rainy) band with a time lag of 7–10 days. Vecchi and Harrison (2002) indicate that this phase relation could be exploited to predict monsoon breaks. The speed of northward movement of SST is the same as that for atmospheric fields but lags behind Q_{net} by about 7 days. The quadrature relationship between SST and Q_{net} indicates that intraseasonal SST fluctuations are essentially being driven by atmospheric ISV through Q_{net}. The quadrature relationship between

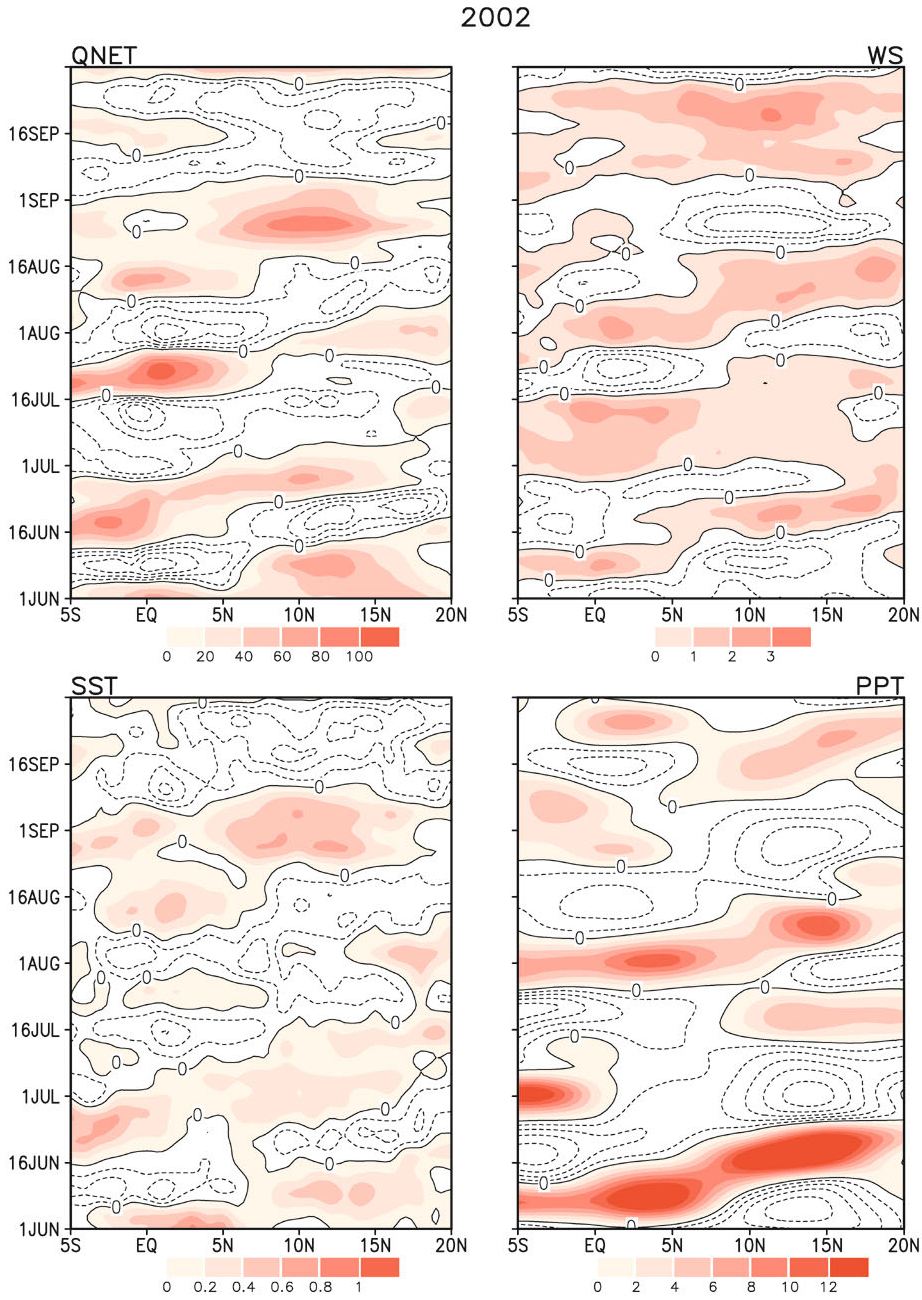

Figure 2.18. Time–latitude section of 10 to 90-day filtered net heat flux (Q_{net}; $W\,m^{-2}$), surface wind speed (WS; $m\,s^{-1}$), SST (°C), and CMAP precipitation (PPT; $mm\,day^{-1}$) for the 2002 summer season averaged over 85°E–90°E. Positive (negative) anomalies are shown with shading (contours). Contour intervals are the same for both positive and negative anomalies.

SST and Q_{net} is not found to hold good over the equatorial IO and the western IO coastal region (Sengupta *et al.*, 2001), where ocean dynamics also seems to play a role in determining SST. Waliser *et al.* (2003b) study an ocean model with a mixed layer using the daily wind stresses and heat fluxes associated with atmospheric ISOs. While the net heat flux associated with ISOs is a major forcing, they found that mixed layer depth (MLD) variations tended to contribute positively to SST variations. Further, contributions from advection and/or entrainment within the Somali Current region and equatorial IO are significant.

From the above discussion, it is clear that atmospheric ISOs do force ISO in SST over the IO. However, the role of intraseasonal fluctuations of SST in determining either the scale selection or northward movement of Asian monsoon ISOs is unclear. Is air–sea coupling crucial for the existence of observed ISOs? Air–sea coupling is certainly important for observed summer ISOs as the quadrature phase relationship between atmospheric convection (or precipitation) and SST cannot be simulated by an AGCM forced by observed daily SST (Wu *et al.*, 2002; Fu *et al.*, 2003). Although intraseasonal variations of SST in this region may act almost like a slave to atmospheric ISV, the coupling between ocean and atmosphere is essential to simulate the correct phase relationship between convection and SST. This was demonstrated by Fu *et al.* (2003) when they coupled an AGCM to a relatively simple ocean model without flux corrections and were able to simulate the observed period, northward movement, and phase relationship between precipitation and SST reasonably well. When the AGCM is forced by daily SST from the coupled run, the AGCM-simulated precipitation band is in phase with SST. Several recent studies (Rajendran *et al.*, 2004; Zheng *et al.*, 2004; Rajendran and Kitoh, 2006; Pegion and Kirtman, 2007) compared simulation of a coupled GCM (CGCM, an AGCM coupled to an OGCM) with simulations of the AGCM forced by CGCM SSTs, and found that the coupling not only improves simulation of the spatial structure of the summer ISOs, but also is essential in simulating the observed quadrature relationship between precipitation and SST. Fu *et al.* (2007) using a hybrid coupled ocean–atmosphere model show that atmospheric ISO forces coherent SST fluctuations in the ocean which in turn provides external forcing for atmospheric ISO, making it more coherent. They further show that such coupling can lead to enhancement of the limit on potential predictability of the ISO by 7 days. Is the air–sea interaction crucial for the existence of summer ISOs? As discussed in Sections 2.1 and 2.2, the theories of atmospheric ISOs indicate that the basic temporal-scale selection and northward propagation of atmospheric summer ISOs arise from internal feedback within the atmosphere. Several AGCMs forced by prescribed SST exhibit ISV levels at or above those found in observations with spatial patterns that resemble the observed pattern (Kemball-Cook and Wang, 2001; Waliser *et al.*, 2003b; Jiang *et al.*, 2004; Klingaman *et al.* 2008; Liu *et al.* 2009) and include some form of northward propagation. This also supports the hypothesis that the basic oscillation and northward propagation may be of internal atmospheric origin. Air–sea interactions can modify these internally triggered oscillations in amplitude, frequency domain, and northward propagation characteristics. Kemball-Cook and Wang (2001) find that air–sea coupling enhances northward propagation of summer

ISOs significantly. Waliser *et al.* (2004) find that air–sea coupling also improves the spacetime characteristics of summer ISOs over the IO. Fu *et al.* (2002) also find that ocean–atmosphere coupling improves simulation of the amplitude and northward propagation characteristics of ISOs. However, some of these results could be influenced by mean state bias of individual components of the coupled model. Therefore, quantitative estimation of modification of summer ISOs by air–sea coupling is still not well established. One particular aspect of the air–sea interaction that is still not clear from all these studies is how the ISV of SST feeds back to the convective activity of the atmosphere and modifies ISO characteristics. Modeling of air–sea interactions associated with northern summer monsoon ISOs is still in its early days. More studies are required to unravel the quantitative role played by the SST in determining the amplitude and phase propagation of monsoon ISOs.

2.4 CLUSTERING OF SYNOPTIC EVENTS BY ISOS

The modulation of synoptic activity by the large-scale circulation anomalies associated with the MJO has been demonstrated by Liebmann *et al.* (1994) and Maloney and Hartmann (2000). The horizontal structure of low-level winds associated with the summer monsoon 30 to 60-day mode (Figure 2.10b) also has large scales and is similar to that of the seasonal mean (Figure 2.1e). Therefore, the meridional shear of low-level zonal winds and cyclonic vorticity at 850 hPa are significantly enhanced (weakened) during an active (break) phase of ISOs. Hence, conditions for cyclogenesis are much more favorable during an active phase than a break phase. Similar to the MJO, do monsoon ISOs modulate synoptic activity in the region during northern summer? Using genesis and track data for low-pressure systems (LPSs) for 40 years (1954–1993), Goswami *et al.* (2003) show that the genesis of an LPS is nearly 3.5 times more favorable during an active condition (147 events corresponding to normalized index $> +1$) than with a break condition (47 events corresponding to normalized index < -1) of monsoon ISOs. They also show that LPSs are spatially strongly clustered to be along the MT region under active conditions (Figure 2.19). Day-to-day fluctuations of precipitation are essentially governed by synoptic activity. As synoptic activity is clustered in time and space by ISOs, a prediction of ISO phases about 3 weeks in advance may allow one to also predict the probability of high (low) rainfall activity with such a lead time. Using daily rainfall data and LPS data during 1901–1970, Krishnamurthy and Shukla (2007) find that seven times more depressions occur during active phases than during break phases. A more detailed analysis of the association between different phases of monsoon ISOs and LPSs has recently been carried out by Krishnamurthy and Ajaya Mohan (2010) using data over a longer period (1901–2003).

Due to the much larger horizontal scale of monsoon ISOs and the MJO compared with that of synoptic disturbances, all these studies (Liebmann *et al.*, 1994; Maloney and Hartmann, 2000; Goswami *et al.*, 2003) argue that the collective effect of randomly occurring synoptic disturbances could not influence the structure of ISOs significantly. However, a recent study by Straub and Kiladis (2003) indicates

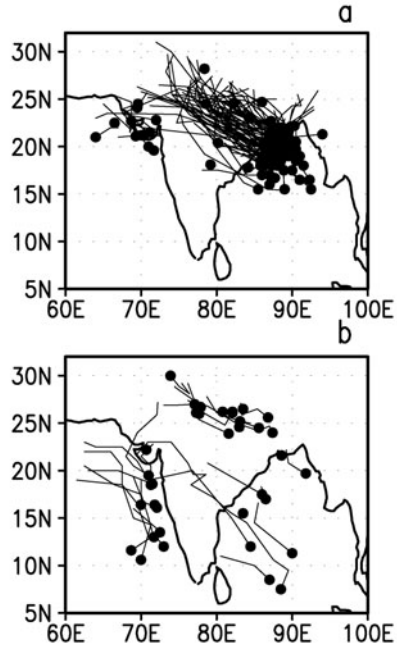

Figure 2.19. Tracks of LPSs for the period 1954–1983 during extreme phases of monsoon ISOs. (a) Active ISO phase (MISI $> +1$) and (b) break ISO phase (MISI > -1). The MISI (monsoon ISO index) used here is the 10 to 90-day filtered relative vorticity during the summer monsoon season (June 1–September 30) averaged over 80°E–95°E and 12°N–22°N. Dark dots represent the genesis point and the lines show their tracks. Large number of LPSs during the active phase are strongly clustered along the MT. The few LPSs that form during breaks clearly avoid the MT region and form either near the foothills of the Himalayas or off the western coast and move westward (after Goswami *et al.*, 2003; © American Geophysical Union).

that westward-propagating mixed Rossby–gravity wave–tropical disturbance (MRG-TD) type synoptic disturbances may have some influence on the structure of summer ISOs.

2.5 MONSOON ISOS AND PREDICTABILITY OF THE SEASONAL MEAN

The prediction of summer monsoon rainfall at least one season in advance is of great importance for the agro-based economy of the region. For over a century, attempts have been made to predict seasonal mean monsoon rainfall using statistical methods involving local and global antecedent parameters that correlate with monsoon rainfall (e.g., Blanford, 1884; Walker, 1923, 1924; Gowarikar *et al.*, 1989; Sahai *et al.*, 2003; Rajeevan *et al.*, 2004). Linear or nonlinear regression models as well as

neural network models (Goswami and Srividya, 1996) indicate a degree of skill when the monsoon is close to normal (about 70% of years over the past 130-year period) but fails to predict the extremes with a level of skill that is useful. Almost all statistical models failed to predict the droughts of 2002, 2004, and 2009. Delsole and Shukla (2002) argue that regression models with many predictors (e.g., the 16-parameter model of the Indian Meteorological Department; Gowarikar *et al.*, 1989) may possess a degree of artificial skill and often regression models with two or three parameters produce better forecasts on average than regression models with multiple predictors. Thus, the usefulness of statistical models is limited. A series of sensitivity studies (Charney and Shukla, 1981; Shukla, 1981, 1987; Lau, 1985) have shown that the tropical climate is, in general, much less sensitive to initial conditions and, hence, more predictable than the extratropical climate. These studies laid the foundation for deterministic climate prediction in the tropics, and dynamical prediction of the seasonal mean monsoon using state-of-the-art climate models appears to be a logical alternative to statistical prediction. Although climate models have improved significantly over the years in simulating mean climate, they still do not have a higher level of skill than statistical models in predicting the seasonal mean monsoon (Kang *et al.*, 2002b; Wang *et al.*, 2004). Almost all present day climate models have serious difficulty in simulating the seasonal mean monsoon climate and its interannual variations (Sperber and Palmer, 1996; Gadgil and Sajani, 1998; Kang *et al.*, 2002a, b; Wang *et al.*, 2004). Even though the climates of certain tropical regions show very little sensitivity to initial conditions (e.g., Shukla, 1987), the Indian summer monsoon appears to be an exception within the tropics and appears to be quite sensitive to initial conditions (Sperber and Palmer, 1996; Sperber *et al.*, 2001; Krishnamurthy and Shukla, 2001), making it probably the most difficult climate system to simulate and predict.

What makes the Indian monsoon such a difficult system to simulate and predict? The sensitivity of the monsoon climate to initial conditions indicates the existence of significant internal low-frequency (LF) variability in the monsoon region (Goswami, 1998). The predictability of the monsoon is going to be determined by the extent to which internal LF variability governs the IAV of the monsoon. What is responsible for such internal LF variability in the monsoon region? We recall (see Section 2.2) that monsoon ISOs arise due to the internal dynamical feedback between organized convection and large-scale circulation with the possibility of SST coupling playing a role. Could monsoon ISOs lead to any significant LF internal variability? If they do, that part of monsoon IAV would be unpredictable. Ajaya Mohan and Goswami (2003) make estimates of the internal IAV of circulation based on daily data from NCEP–NCAR reanalysis for more than 40 years and convection data for more than 20 years, and show that almost all internal IAV in the tropics arises from ISOs. Hoyos and Webster (2007) also find that a proportion of the interannual modulation of monsoon rainfall is the direct result of the cumulative effect of rainfall variability on intraseasonal (25–80 day) timescales.

How do ISOs influence the seasonal mean and its IAV? We noted in Section 2.1.2 that the spatial structure of the 30 to 60-day mode (Figure 2.10) is similar to that of the seasonal mean (Figure 2.1), strengthening (weakening) the seasonal mean

in its active (break) phases. As shown in Figure 2.20, the ISV and IAV of the Asian monsoon are, in fact, governed by a common spatial mode of variability (Fennessy and Shukla, 1994; Ferranti *et al*., 1997; Goswami *et al*., 1998; Goswami and Ajaya Mohan, 2001; Goswami and Xavier, 2005). As the horizontal structures of ISOs and the seasonal mean are similar, there is a higher probability of active (break) conditions within a season resulting in a stronger (weaker) than normal monsoon. If monsoon ISOs were a single-frequency sinusoidal oscillation, this could not happen. However, due to the existence of a band of frequencies, ISOs are rather quasi-periodic and hence there is ahigher probability of active (break) phases within a season taking place. Goswami and Ajaya Mohan (2001) and Goswami *et al*. (2006) show that a strong (weak) Indian monsoon is associated with the higher probability of occurrence of active (break) conditions. Sperber *et al*. (2000) also show that the ISV and IAV of the Asian monsoon are governed by a common mode of spatial variability and that strong (weak) monsoons are associated with a higher probability of occurrence of active (break) conditions. In a series of interesting studies, Krishnamurthy and Shukla (2007, 2008) examine how ISOs influence the seasonal mean and—using multi-channel singular spectrum analysis—were able to separate the seasonally persisting component of ISV that influences the seasonal mean. Further work is required to elucidate the origin of the seasonally persisting component of ISV. Is it a result of nonlinear interaction between the oscillatory components of ISV as well as of higher frequency oscillation? Or, is it driven by some slowly varying external forcing? The fact that ISV influences the seasonal mean and its predictability is a conclusion reached by Waliser *et al*. (2003b), who compare simulation of the seasonal mean and ISV using a number of AGCMs and find that higher ISV is associated with higher intra-ensemble variance (internal variability) and poorer predictability of the seasonal mean.

The predictability of the seasonal mean monsoon is governed by the relative contribution of slowly varying external components of forcing (such as that associated with the ENSO) and internal variability to the observed IAV of the monsoon. High (low) predictability is associated with a higher (lower) contribution of external forcing to the IAV than that from internal variability. How much of the total IAV of the Asian monsoon is actually governed by LF internal variability? Estimates made using AGCMs (Goswami, 1998; Goswami and Xavier, 2005) and using long observations (Ajaya Mohan and Goswami, 2003) indicate that about 50% of the total IAV of the Asian monsoon is governed by the internal component coming primarily from ISOs. Thus, ISOs make the Asian monsoon a difficult system to predict by making the unpredictable noise comparable with the externally forced predictable signal. For many years, a consensus on the fraction of total IAV of the Indian monsoon governed by ISOs was lacking. However, a consensus towards what is concluded here is slowly evolving. Therefore, the seasonal mean summer monsoon will remain a difficult system to predict. Clever methods will have to be devised to simulate and identify the weak signal from a background of noise of comparable amplitude. The prospect of predicting the seasonal mean monsoon would have improved if the statistics of summer ISOs were strongly modulated (or constrained) by slowly varying forcing (such as that associated with the ENSO). Modeling studies

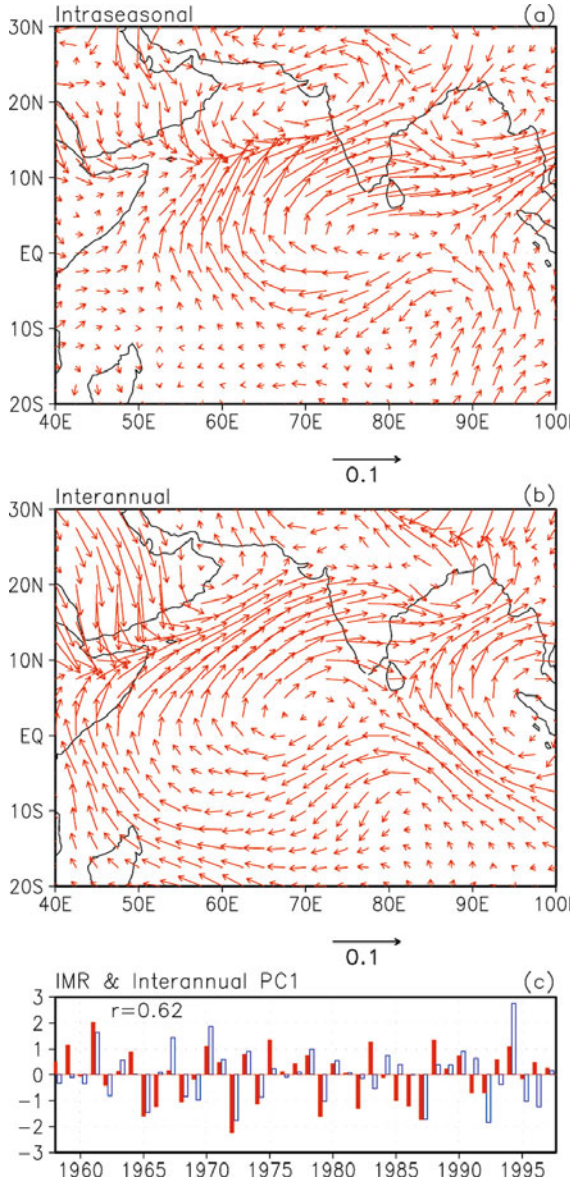

Figure 2.20. First EOF of intraseasonal and interannual 850 hPa winds. (a) Intraseasonal EOFs are calculated using ISO-filtered winds for the summer months (June 1–September 30) for a period of 20 years (1978–1997). (b) Interannual EOFs are calculated using seasonal mean (JJAS) winds for a 40-year period (1958–1997). The units of vector loading are arbitrary. (c) Relation between all India monsoon rainfall (IMR; unfilled bars) and interannual PC1 (filled bar). Both time series are normalized by their own standard deviation. Correlation between the two time series is shown ((a) and (b) are from Goswami and Ajaya Mohan, 2001; (c) is copyright © of the American Meteorological Society).

so far, however, indicate that summer monsoon ISOs over the Asian monsoon region are not sufficiently influenced by the slowly varying SST changes associated with the ENSO.

2.6 AEROSOLS AND MONSOON ISOS

An emerging area of interest is the interaction between aerosols and monsoon ISOs (MISOs). The Asian monsoon region is known to have high concentrations of natural as well as anthropogenic aerosols that significantly influence the regional climate through direct radiative forcing (Jayaraman, 2001; Pandithurai *et al*., 2008; Ramanathan and Carmichael, 2008). Some studies (Ramanathan *et al*., 2005) indicate that aerosols may lead to weakening of the seasonal mean Indian monsoon through cooling the land and weakening the north–south surface temperature gradient. Some other studies (e.g., Lau *et al*. 2006), on the other hand, indicate that—due to the absorbing nature of some aerosols—the Indian monsoon may strengthen through the elevated heat pump mechanism. While considerable attention has been paid to address how aerosols may influence the seasonal mean monsoon (Meehl *et al*., 2008; Collier and Zhang, 2009), not many studies have addressed the issue of how aerosols might influence monsoon ISOs and vice versa. There is, however, the basis to think that aerosols and MISOs may interact with each other. MISOs can give rise to significant oscillation of aerosol concentrations as a result of the washout effect during active phases and to accumulation and buildup during break phases. In addition to surface cooling over land during a break phase, warming of the atmosphere in the 1 km to 3 km layer due to absorbing aerosols could affect the stability of the atmosphere and influence the transition to active phase and, hence, the periodicity of MISOs.

In a recent study, Manoj *et al*. (2011) show that the aperiodicity of MISOs—associated with the fact that some long breaks go over to an active spell while many other long breaks do not transit to an active spell—may be related to an interaction between absorbing aerosols and ISO circulation. It is shown that breaks that are followed by active conditions (BFA cases) are characterized by a much higher concentration of absorbing aerosols (AI index) compared with breaks that are not followed by active (BNFA cases) conditions (Figure 2.21a–c). The circulation associated with BFA allows desert dust to be transported (see Manoj *et al*., 2011) and helps the accumulation of locally generated absorbing aerosols (such as black carbon) while that associated with BNFA cases not only does not allow transport from west to northwest but also allows the locally generated aerosols to be transported out of central India (Figure 2.21d–f). The difference in the circulation in the two types of breaks is that in the BNFA cases there is increased organized convection over eastern India, Myanmar, the south China Sea and Southern China (Figure 2.21f). Manoj *et al*. (2011) show that heating of the 1 km to 3 km layer by absorbing aerosols in BFA cases compared with the pristine region over the equatorial Indian Ocean culminates in a significant north–south temperature gradient resulting in strong low-level moisture transport to central India that is able to overcome the

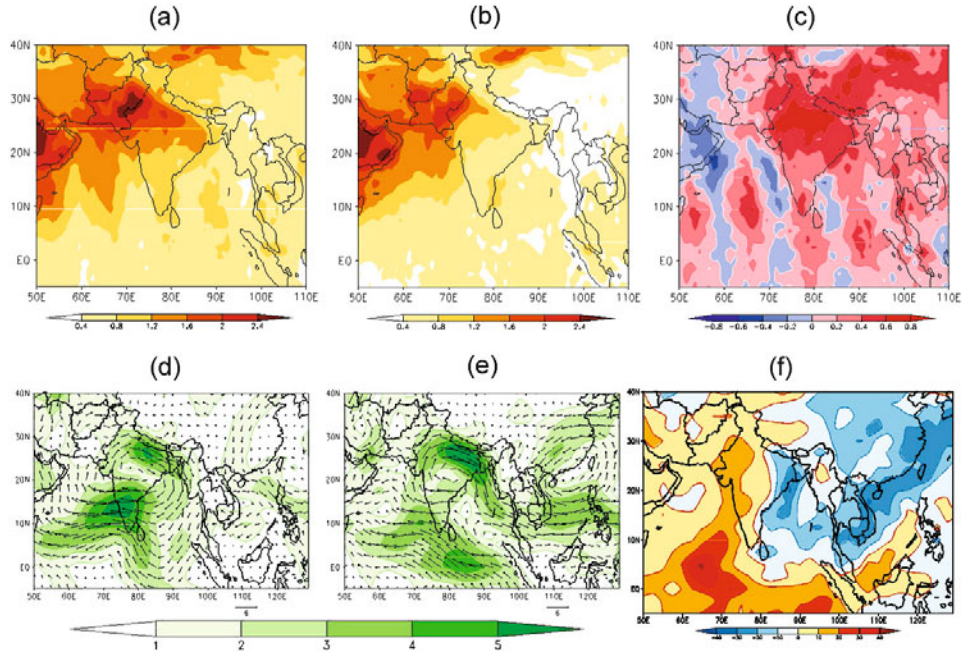

Figure 2.21. (a) Composite AI index for BFA cases. (b) Composite AI index for BNFA cases. (c) Difference between BFA and BNFA composite AI index. (d) Same as (a) but for 850 hPa winds. (e) Same as (b) but for 850 hPa winds. (f) Difference of OLR ($W\,m^{-2}$) composites between BFA and BNFA cases (BFA – BNFA).

stability effect and facilitate a quick transition to an active phase. In BNFA cases, stability cannot be overcome easily due to lack of such a temperature gradient and low-level moisture transport. This demonstration that aerosols are intrinsically linked with transitions of MISOs indicates that thermodynamically active aerosols must be included in any comprehensive theory and prediction of MISOs.

2.7 PREDICTABILITY AND PREDICTION OF MONSOON ISOS

While monsoon ISOs make the seasonal mean monsoon difficult to predict, they themselves may possess predictability beyond the current skill of medium-range prediction by virtue of their quasi-periodic nature. Prediction of long dry spells 2 to 3 weeks in advance is important to farmers when planning sowing, harvesting, and water management. What is the limit on the prediction of dry and wet spells or break and active phases of monsoon ISOs? These and other issues related to predictability and extended range prediction of summer monsoon ISOs are discussed at length in Chapter 12 and, hence, will not be repeated here. Two important findings are summarized here. The first finding is that the potential predictability of monsoon

breaks is much higher than that for monsoon active conditions (Goswami and Xavier, 2003; Waliser *et al*., 2003a). Second, simple empirical models developed during the last couple of years (Goswami and Xavier, 2003; Webster and Hoyos, 2004) demonstrate a potential for predicting summer monsoon ISOs up to 3 weeks in advance. A limitation of some of these empirical models was that they were not suitable for real time predictions due to endpoint problems arising from the use of some form of time filters. The development of analogue models for real time forecasting of summer monsoon ISOs with a level of skill that is useful up to 3 weeks in advance (Xavier and Goswami, 2007; Chattopadhyay *et al*., 2008) during the past couple of years may be considered a major advance in this direction. These developments in the real time prediction of summer ISOs as well as of the MJO are reviewed in Goswami *et al*. (2011).

2.8 SUMMARY AND DISCUSSION

A synthesis of the large-scale spatial and temporal structure and regional propagation characteristics of Asian summer monsoon ISV is presented in this chapter, based on advances made in global observations. Such observations have revealed that the active and break phases of the SA monsoon or the wet and dry spells over the Indian continent are manifestations of the superposition of 10 to 20-day and 30 to 60-day oscillations. Both the 10 to 20-day oscillation and the 30 to 60-day oscillation contribute roughly equally to total ISV in the SA monsoon region. While 30 to 60-day oscillation has a very large zonal scale encompassing both the SA and the EA/WNP monsoon regions, the 10 to 20-day oscillation has a smaller zonal scale and is regional in character. The 30 to 60-day mode is characterized by northward propagation while the 10 to 20-day mode is characterized by westward propagation. The ISV on a 30 to 60-day timescale over the EA/WNP region (see Chapter 3) and that over the SA region are closely related through the evolution (northward propagation) of the large spatial structure associated with the 30 to 60-day mode. Also the 10 to 20-day variability over the SA region is associated with the 10 to 20-day oscillation propagating from the western Pacific and amplification over the BoB. Thus, ISVs over the SA and EA/WNP monsoon regions are intimately related.

Advances made in understanding the scale selection for the 30 to 60-day mode and its northward propagation and that for the 10 to 20-day mode and its westward propagation are reviewed based on an analysis of observations and a hierarchy of modeling studies. Two mechanisms seem to contribute to the temporal-scale selection of the 30 to 60-day mode. One is a ''convection–thermal relaxation feedback mechanism'', according to which convective activity results in an increase of static stability which depresses convection itself. As convection dies, dynamical processes and radiative relaxation decrease moist static stability and bring the atmosphere to a new convectively unstable state. This mechanism does not involve wave dynamics and may be responsible for northward-propagating 30 to 60-day oscillations not associated with the eastward propagation of convection in

the equatorial region. The other mechanism involves the eastward propagation of convection over the equatorial IO in the form of a Kelvin wave and west to northwest propagation of Rossby waves emanated over the western Pacific. The timescale is determined in this case by the propagation time of the moist Kelvin wave from the eastern IO to the western Pacific and the moist Rossby waves from the western Pacific to the AS where they decay and a new equatorial perturbation is generated.

An important advance has also been made in understanding the poleward propagation of the 30 to 60-day mode. Several modeling studies have indicated that the ground hydrology and meridional gradient of moist static stability were important for the northward propagation of the mode. However, a clear physical picture has not emerged. Some diagnostic studies then showed that low-level relative vorticity drives boundary layer moisture convergence that is maximum about 3°N of the convection maximum. What is responsible for low-level vorticity to be maximum about 3°N of the convection maximum has been elucidated in some recent modeling and theoretical studies. The easterly vertical shear of summer mean flow couples the barotropic and baroclinic components of response to convective heating and generates a barotropic vorticity maximum north of the convection maximum. The barotropic vorticity maximum forces boundary layer moisture convergence to be maximum to the north of the heating maximum. Thus, a better understanding is emerging for mean northward propagation. However, we recall that northward propagation is rather intermittent within a summer season and varies from year to year. For the predictability of ISO phases, we need to understand the cause of the variability of northward propagation of the 30 to 60-day mode. This is still an important outstanding problem and more theoretical and modeling work is required in this direction.

Another major advance has been made in understanding the genesis and scale selection of the 10 to 20-day mode. Until recently, no clear physical mechanism for selection of the 10 to 20-day mode period, wavelength, and westward phase propagation was known. A unified model now explains the spatial structure (wavelength), period, and westward phase speed of both summer and winter 10 to 20-day oscillations or the QBM. It is demonstrated that the QBM is an $n = 1$ equatorial Rossby wave, with a wavelength about 6,000 km and a period of 14–16 days, which is shifted to the north (south) of the equator by about 5° by summer (winter) background mean flow (Chatterjee and Goswami, 2004). For some time, the driving mechanism for the observation of equatorial Rossby waves with a 10 to 20-day timescale was a puzzle, as some theoretical studies indicated that convective feedback could not make the $n = 1$ equatorial Rossby mode unstable. A recent study (Chatterjee and Goswami, 2004) shows that inclusion of a proper boundary layer (inclusion of turbulent entrainment) allowed the $n = 1$ equatorial Rossby mode to become unstable with a maximum growth rate corresponding to the observed period and wavelength.

The interaction between the ocean and the atmosphere on intraseasonal timescales during the northern summer and its role in the scale selection and northward propagation of monsoon ISOs are also reviewed. This is an area where

our knowledge has just begun to grow. Two things became clear during the last couple of years. A reasonable estimate of ISV of net heat flux at the surface (made possible by the availability of reliable SST from TMI, surface winds from QuikSCAT, and NOAA OLR on daily timescales) showed that ISV of heat flux is a major driving force for the ISV of SST over most of the tropical IO, although advection and entrainment play roles in the equatorial IO and the Somali Current region. It is also noted that there exists a quadrature phase relationship between the northward propagation of SST and precipitation on the 30 to 60-day timescale and that air–sea coupling is crucial for this observed phase relationship between SST and precipitation. Thus, atmospheric ISOs seem to lead to ISOs in SST (largely through heat fluxes) and the air–sea coupling is certainly required for the observed phase relationship between SST and precipitation. However, it is still unclear how ISOs in SST feed back to ISOs in convection and modify them. It appears that the basic genesis, temporal-scale selection, and northward phase propagation may arise from atmospheric internal dynamics and that air–sea coupling modifies the spatio-temporal character in some way. However, the quantitative contribution of air–sea coupling to spacetime spectra and northward propagation is not well settled at this time. Much more theoretical and modeling work is required to resolve these issues.

Developing coupled ocean–atmosphere GCMs for the Asian monsoon region is a challenging task, although some initial work is being made. This is because almost all AGCMs have large systematic errors in simulating mean SA monsoon and most OGCMs have more than a 1°C error in simulating mean SST over the IO. These systematic errors of component models lead to a drift of the coupled model climate that may influence the quantitative estimates sought above. However, the following observation provides a silver lining. We note that the signal in SST fluctuations on the intraseasonal timescale (1°C) is larger than that on the interannual timescale (0.5°C) during northern summer over the IO. Also, the amplitude of the dominant forcing—namely, net surface heat flux—on the intraseasonal timescale (60–80 $W m^{-2}$) is much larger than that on the interannual timescale.

The interactions between summer monsoon ISOs and various scales of motion have also been summarized. What started in the mid 1970s (Dakshinamurthy and Keshavamurthy, 1976; Alexander *et al.*, 1978) and the early 1980s (Yasunari, 1979; Sikka and Gadgil, 1980) as innocuous quasi-periodic oscillations that contribute to the active and break spells within the monsoon season, has now developed into the ISOs of the SA monsoon emerging as a major building block of the SA monsoon itself. On the one hand, they produce spacetime clustering of the synoptic disturbances (lows and depressions) and control the day-to-day fluctuations of precipitation while, on the other hand, they influence the seasonal mean and contribute significantly to the IAV of seasonal mean precipitation. It is estimated that modulation of the seasonal mean monsoon by slowly varying external forcing is rather weak and up to 50% of the total IAV may be contributed by internal variability arising from monsoon ISOs. This leads to poor predictability of the seasonal mean SA monsoon, as ISOs are primarily of internal atmospheric origin and the component of IAV of the seasonal mean contributed by ISOs may be unpredictable. The potential predictability of the monsoon would have been enhanced if the statistics of ISOs were also

modulated by slowly varying external forcing. Currently available studies indicate that ISO statistics over the Asian monsoon region is only weakly modulated by slowly varying SST forcing. However, we now know that air–sea coupling is involved in the ISV of the SA monsoon. Coupled evolution of SST and circulation and precipitation on the intraseasonal timescale may introduce certain constraints on the internal variability generated by ISOs. However, this question is just being raised and no study has addressed it so far. In the coming years, CGCMs should investigate whether predictability of the seasonal mean monsoon is enhanced by air–sea coupling of summer monsoon ISOs. Monsoon predictability could also be influenced by interdecadal variability of external forcing and interdecadal variability of ISO statistics. The role of ISOs in the interdecadal variability of predictability of the SA monsoon needs to be studied using long observations and coupled models.

Exploiting the quasi-periodic nature of ISOs, it has been shown (Goswami and Xavier, 2003; Webster and Hoyos, 2004; Xavier and Goswami, 2007; Chattopadhyay *et al*., 2008) that the phases of ISOs could be predictable up to 3 weeks in advance. This knowledge is likely to be put to practical use in extended range forecasting of the dry and wet spells of the monsoon and flood forecasting. Improvement in the extended range forecasting of ISO phases, however, may come only from better understanding and simulation of within-season and year-to-year variability of northward-propagating events. Fundamental work is required to advance the understanding of this aspect of ISOs.

For better long-range prediction of the seasonal mean and for better extended range prediction of ISOs themselves, it is apparent that CGCMs must simulate the climatology of ISOs correctly. However, ISOs do influence the annual cycle, and ISO activity is related to the internal variability of the seasonal mean. Waliser *et al*. (2003b) find that AGCMs with higher (lower) internal variability are associated with a stronger (weaker) annual cycle. Thus, ISO activity may be indirectly tied to the hydrological cycle of a model. The hydrological cycle of a model, in turn, depends on various parameterizations of the model, such as the cumulus scheme, land surface processes, etc. Model-to-model variability in simulating the statistics of ISOs may be related to differences in these parameterization schemes. Correct simulation of the climatology of observed ISOs, therefore, remains a challenging task and continued focused efforts must be made to improve summer ISO simulations in GCMs.

2.9 ACKNOWLEDGMENTS

This work was partially supported by the Department of Ocean Development, Government of India and the Indian National Centre for Ocean Information Services (INCOIS), Hyderabad. I thank D. Sengupta for his comments on the draft of this manuscript. I am grateful to Duane, Bill, and an anonymous reviewer for detailed and constructive comments that significantly improved the presentation of the chapter. Some of the results presented in the chapter grew out of work done in collaboration with my colleague D. Sengupta and students R. S. Ajaya Mohan,

Retish Senan, and Prince Xavier. I am thankful to Prince Xavier, Neena Mani Joseph, and E. Suhas for help in preparing the manuscript.

2.10 APPENDIX

Several datasets have been utilized in preparing the figures presented in this chapter. Primary among them are the daily circulation data from NCEP–NCAR reanalysis (Kalnay *et al*., 1996; Kistler *et al*., 2001), daily interpolated outgoing longwave radiation (OLR) data (Liebmann and Smith, 1996), and daily precipitation estimates from GPCP (Huffman *et al*. 2001). We have also used high-resolution daily rainfall data over India compiled by the India Meteorological Department (Rajeevan *et al*., 2006) based on 1,803 stations distributed over the country. For the large-scale pattern of precipitation climatology, we have used CMAP data (Xie and Arkin, 2006). NCEP–NCAR reanalysis, interpolated OLR, and CMAP precipitation are available at $2.5^\circ \times 2.5^\circ$ horizontal resolution. The daily precipitation from GPCP (Huffman *et al*., 2001) and IMD are available at $1^\circ \times 1^\circ$ horizontal resolution. Daily anomalies are constructed as deviations from daily observations from an annual cycle defined as the sum of the annual mean and the first three harmonics. To extract bandpass-filtered data we have generally used a Lanczos filter (Duchon, 1979). The surface winds and SST were obtained from the microwave imager on board the TRMM satellite (Wentz *et al*., 2000) and were not affected by clouds, aerosols, and atmospheric water vapor. A 3-day running mean provided data at $0.25^\circ \times 0.25^\circ$ horizontal resolution.

2.11 REFERENCES

Abrol, Y. P. and S. Gadgil (Eds.) (1999) *Rice in a Variable Climate*. APC Publications, New Delhi, 243 pp.

Ajaya Mohan, R. S. and B. N. Goswami (2003) Potential predictability of the Asian summer monsoon on monthly and seasonal time scales. *Meteorol. Atmos. Phys*., doi: 10.1007/s00703-002-0576-4.

Ajaya Mohan, R. S. and B. N. Goswami (2007) Dependence of simulation of boreal summer tropical intraseasonal oscillations on the simulation of seasonal mean. *J. Atmos. Sci*., **64**, 460–478.

Ajaya Mohan, R. S., H. Annamalai, Jing-Jia Luo, J. Hafner, and T. Yamagata (2010) Poleward propagation of boreal summer intraseasonal oscillations in a coupled model: Role of internal processes, *Climate Dynamics*, doi: 10.1007/s00382-010-0839-6.

Alexander, G., R. Keshavamurty, U. De, R. Chellapa, S. Das, and P. Pillai (1978) Fluctuations of monsoon activity. *J. Meteorol. Hydrol. Geophys*., **29**, 76–87.

Ananthakrishnan, R. and M. Soman (1988a) The onset of the south-west monsoon over Kerala: 1901–1980. *J. Climatol*., **8**, 283–296.

Ananthakrishnan, R. and M. Soman (1988b) Onset dates of the south-west monsoon over Kerala for the period 1870–1900. *Int. J. Climatol*., **9**, 321–322.

Ananthakrishnan, R., U. R. Acharya, and A. R. R. Krishnan (1967) *On the Criteria for Declaring the Onset of the Southwest Monsoon over Kerala* (forecasting manual, FMU Rep. No. IV-18.1). India Meteorological Department, Pune, India, 52 pp.

Annamalai, H. and J. M. Slingo (2001) Active/break cycles: Diagnosis of the intraseasonal variability of the Asian summer monsoon. *Climate Dynamics*, **18**, 85–102.

Bellon, J. and J. Srinivasan (2006) Comments on "Structures and mechanisms of the northward propagating boreal summer intraseasonal oscillation." *J. Climate*, **19**, 4738– 4743.

Bhat, G., S. Gadgil, S. Kumar, P. V. Hareesh Kalsi, S. R. Madhusoodanan, P. Murty, V. S. N. Prasada Rao, C. V. K. Babu, and V. Ramesh Rao (2001) BOBMEX: The Bay of Bengal monsoon experiment. *Bull. Amer. Meteorol. Society*, **82**, 2217–2243.

Blanford, H. F. (1884) On the connection of the Himalaya snowfall with dry winds and seasons of drought in India. *Proc. Royal Society London*, **37**, 3–22.

Blanford, H. F. (1886) Rainfall of India. *Mem. India Meteorol. Department*, **2**, 217–448.

Charney, J. G. and J. Shukla (1981) Predictability of monsoons. In: J. Lighthill and R. P. Pearce (Eds.), *Monsoon Dynamics*. Cambridge University Press, Cambridge, U.K., pp. 99–108.

Chatterjee, P. and B. N. Goswami (2004) Structure, genesis and scale selection of the tropical quasi-biweekly mode. *Quart. J. Roy. Meteorol. Soc.*, **130**, 1171–1194.

Chattopadhyay, R., A. K. Sahai, and B. N. Goswami (2008) Objective identification of nonlinear convectively coupled phases of monsoon intraseasonal oscillation: Implications for prediction. *J. Atmos. Sci.*, **65**, 1549–1569.

Chen, T.-C. and J.-M. Chen (1993) The 10–20-day mode of the 1979 indian monsoon: Its relation with the time variation of monsoon rainfall. *Mon. Wea. Rev.*, **121**, 2465–2482.

Collier, J. C. and G. J. Zhang (2009) Aerosol direct forcing of the summer Indian monsoon as simulated by the NCAR cam3. *Climate Dynamics*, **32**, 313–332.

Dakshinamurthy, J. and R. N. Keshavamurthy (1976) On oscillations of period around one month in the Indian summer monsoon. *Ind. J. Meteorol. Geophys.*, **27**, 201–203.

Delsole, T. and J. Shukla (2002) Linear prediction of Indian monsoon rainfall. *J. Climate*, **15**(24), 3645–3658.

Drbohlav, H. K. L. and Bin Wang (2005) Mechanism of the northward-propagating intraseasonal oscillation: Insights from a zonally symmetric model. *J. Climate*, **18**, 952–972

Duchon, C. (1979) Lanczos filtering in one and two dimensions. *J. Appl. Meteorol.*, **18**, 1016–1022.

Fennessy, M. and J. Shukla (1994) Simulation and predictability of monsoons. Paper presented at *Proceedings of the International Conference on Monsoon Variability and Prediction, WMO/TD619, Trieste*, pp. 567–575.

Ferranti, L., J. M. Slingo, T. N. Palmer, and B. J. Hoskins (1997) Relations between interannual and intraseasonal monsoon variability as diagnosed from AMIP integrations. *Quart. J. Roy. Meteorol. Soc.*, **123**, 1323–1357.

Flatau, M., P. Flatau, and D. Rudnick (2001) The dynamics of double monsoon onsets. *J. Climate*, **14**, 4130–4146.

Flatau, M., P. Flatau, J. Schmidt, and G. Kiladis (2003) Delayed onset of the 2002 Indian monsoon. *Geophys. Res. Lett.*, **30**(14), 1768, doi: 10.1029/2003GL017,434.

Fu, X., B. Wang, and T. Li (2002) Impacts of air–sea coupling on the simulation of mean Asian summer monsoon in the ECHAM4 model. *Mon. Wea. Rev.*, **130**, 2889–2904.

Fu, X., B. Wang, T. Li, and J. McCreary (2003) Coupling between northward propagating, intraseasonal oscillations and sea-surface temperature in the Indian ocean. *J. Atmos. Sci.*, **60**(15), 1755–1753.

Fu Xiouhua, Bin Wang, D. E. Waliser, and Li Tao (2007) Impact of atmosphere–ocean coupling on the predictability of monsoon intraseasonal oscillations. *J. Atmos. Sci.*, **64**, 157–174.

Fukutomi, Y. and T. Yasunari (1999) 10–25 day intraseasonal variations of convection and circulation over east Asia and western north Pacific during early summer. *J. Meteorol. Soc. Japan*, **77**(3), 753–769.

Gadgil, S. (1995) Climate change and agriculture: An Indian perspective. *Curr. Sci.*, **69**, 649–659.

Gadgil, S. (2003) The Indian monsoon and its variability. *Annu. Rev. Earth Planet. Sci.*, **31**, 429–467.

Gadgil, S. and P. R. S. Rao (2000) Famine strategies for a variable climate: A challenge. *Curr. Sci.*, **78**, 1203–1215.

Gadgil, S. and S. Sajani (1998) Monsoon precipitation in the AMIP runs. *Climate Dynamics*, **14**, 659–689.

Gadgil, S. and J. Srinivasan (1990) Low frequency variation of tropical convergence zone. *Meteorol. Atmos. Phys.*, **44**, 119–132.

Gill, A. E. (1980) Some simple solutions for heat-induced tropical circulation. *Quart. J. Roy. Meteorol. Soc.*, **106**, 447–462.

Gill, A. E. (1982) *Atmosphere–Ocean Dynamics* (Vol. 30 of International Geophysics Series). Academic Press, San Diego, CA, 666 pp.

Goswami, B. N. (1994) Dynamical predictability of seasonal monsoon rainfall: Problems and prospects. *Proc. Ind. Nat. Acad. Sci.*, **60A**, 101–120.

Goswami, B. N. (1998) Interannual variations of Indian summer monsoon in a GCM: External conditions versus internal feedbacks. *J. Climate*, **11**, 501–522.

Goswami, B. N. and R. S. Ajaya Mohan (2001) Intraseasonal oscillations and interannual variability of the Indian summer monsoon. *J. Climate*, **14**, 1180–1198.

Goswami, B. N. and J. Shukla (1984) Quasi-periodic oscillations in a symmetric general circulation model. *J. Atmos. Sci.*, **41**, 20–37.

Goswami, B. N. and P. Xavier (2003) Potential predictability and extended range prediction of Indian summer monsoon breaks. *Geophys. Res. Lett.*, **30**(18), 1966, doi: 10.1029/2003GL017,810.

Goswami, B. N. and P. K. Xavier (2005) Dynamics of "internal" interannual variability of the Indian summer monsoon in a GCM. *J. Geophys. Res.*, **110**, D24104, doi: 10.1029/2005JD006042.

Goswami, B. N., J. Shukla, E. Schneider, and Y. Sud (1984) Study of the dynamics of the intertropical convergence zone with a symmetric version of the GLAS climate model. *J. Atmos. Sci.*, **41**, 5–19.

Goswami, B. N., D. Sengupta, and G. Sureshkumar (1998) Intraseasonal oscillations and interannual variability of surface winds over the Indian monsoon region. *Proc. Ind. Acad. Sci. (Earth and Planetary Sciences)*, **107**, 45–64.

Goswami, B. N., R. S. Ajaya Mohan, P. K. Xavier, and D. Sengupta (2003) Clustering of low pressure systems during the Indian summer monsoon by intraseasonal oscillations. *Geophys. Res. Lett.*, **30**, 8, doi: 10.1029/2002GL016,734.

Goswami, B. N., G. Wu, and T. Yasunari (2006) The annual cycle, intraseasonal oscillations, and roadblock to seasonal predictability of the Asian summer monsoon. *J. Climate*, **19**, 5078–5098.

Goswami, B. N., M. C. Wheeler, J. C. Gottschalck, and D. E. Waliser (2011) Intraseasonal variability and forecasting: A review of recent research. In: C. P. Chang *et al.* (Eds.), *The Global Monsoon System: Research and Forecast*, Second Edition, World Scientific, Singapore, Ch. 23, pp. 389–409

Goswami, P. and V. Mathew (1994) A mechanism of scale selection in tropical circulation at observed intraseasonal frequencies. *J. Atmos. Sci.*, **51**, 3155–3166.

Goswami, P. and Srividya (1996) A novel neural network design for long-range prediction of rainfall pattern. *Curr. Sci.*, **70**, 447–457.

Gowarikar, V., V. Thapliyal, R. P. Sarker, G. S. Mandel, and D. R. Sikka (1989) Parametric and power regression models: New approach to long range forecasting of monsoon rain in India. *Mausam*, **40**, 125–130.

Hastenrath, S. and P. Lamb (1979) *Climatic Atlas of the Indian Ocean, Part I: Surface Climate Atmosphere Circulation*. University of Wisconcin Press, Madison.

Held, I. and A. Hou (1980) Nonlinear axially symmetric circulations in a nearly inviscid atmosphere. *J. Atmos. Sci.*, **37**, 515–533.

Hendon, H. and M. Salby (1994) The life cycle of Madden–Julian Oscillation. *J. Atmos. Sci.*, **51**, 2207–2219.

Hoyos, C. D. and P. J. Webster (2007) The role of intraseasonal variability in the nature of Asian monsoon precipitation. *J. Climate*, **20**, 4402–4424.

Hsu, H.-H. and C.-H. Weng (2001) Northwestward propagation of the intraseasonal oscillation in the western north Pacific during the boreal summer: Structure and mechanism. *J. Climate*, **14**, 3834–3850.

Huffman, G. J., R. F. Adler, M. Morrissey, D. T. Bolvin, S. Curtis, R. Joyce, B. McGavock, and J. Susskind (2001) Global precipitation at one-degree daily resolution from multi-satellite observations. *J. Hydrometeorol.*, **2**, 36–50.

Jayaraman, A. (2001) Aerosol radiation cloud interactions over the tropical Indian Ocean prior to the onset of the summer monsoon. *Curr. Sci.*, **81**(11), 1437–1445.

Jiang, X., T. Li, and B. Wang (2004) Structures and mechanisms of the northward propagation boreal summer intraseasonal oscillation. *J. Climate*, **17**, 1022–1039.

Jones, C., L. M. V. Carvalho, R. W. Higgins, D. E. Waliser, and J. K. E. Schemm (2004) Climatology of tropical intraseasonal convective anomalies: 1979–2002. *J. Climate*, **17**, 523–539.

Joseph, P., J. Eischeid, and R. Pyle (1994) Interannual variability of the onset of the Indian summer monsoon and its association with atmospheric features, El Nino and sea surface temperature anomalies. *J. Climate*, **7**, 81–105.

Joseph, S., A. K. Sahai, and B. N. Goswami (2009) Eastward propagating MJO during boreal summer and Indian monsoon droughts. *Climate Dynamics*, **32**, doi: 10.1007/s00382-008-0412-8, pp. 1139–1153.

Kalnay, E., M. Kanamitsu, R. Kistler, W. Collins, D. Deaven, L. Gandin, M. Iredell, S. Saha, G. White, J. Woollen *et al.* (1996) The NCEP/NCAR 40-year reanalysis project. *Bull. Amer. Meteorol. Society*, **77**, 437–471.

Kang, I.-S., K. Jin, K.-M. Lau, J. Shukla, V. Krishnamurthy, S. D. Schubert, D. E. Waliser, W. Stern, V. Satyan, A. Kitoh *et al.* (2002a) Intercomparison of GCM simulated anomalies associated with the 1997–98 El Nino. *J. Climate*, **15**, 2791–2805.

Kang, I.-S., K. Jin, B. Wang, K.-M. Lau, J. Shukla, V. Krishnamurthy, S. D. Schubert, D. E. Waliser, W. Stern, V. Satyan, *et al.* (2002b) Intercomparison of the climatological variations of Asian summer monsoon precipitation simulated by 10 GCMs. *Climate Dyn.*, **19**, 383–395.

Kemball-Cook, S. R. and B. Wang (2001) Equatorial waves and air–sea interaction in the boreal summer intraseasonal oscillation. *J. Climate*, **14**, 2923–2942.

Keshavamurthy, R. N., S. V. Kasture, and V. Krishnakumar (1986) 30–50 day oscillation of the monsoon: A new theory. *Beitr. Phys. Atmo.*, **59**, 443–454.

Kistler, R., W. Collins, S. Saha, G. White, J. Woollen, E. Kalnay, M. Chelliah, W. Ebisuzaki, M. Kanamitsu, V. Kousky *et al*. (2001) The NCEP–NCAR 50-year reanalysis: Monthly means CD-ROM and documentation. *Bull. Amer. Meteorol. Society*, **82**, 247–267.

Kikuchi, K. and Bin Wang (2009) Global perspectives of the quasi biweekly oscillation. *J. Climate*, **22**, 1340–1359.

Klingaman, N. C., P. M. Inness, H. Weller, and J. M. Slingo (2008) The importance of high-frequency sea surface temperature variability to the intraseasonal oscillation of Indian monsoon rainfall. *J. Climate*, **21**, 6119–6140.

Knutson, T. and K. Weickmann (1987) 30–60 day atmospheric oscillations: Composite life cycles of convection and circulation anomalies. *Mon. Wea. Rev.*, **115**, 1407–1436.

Knutson, T. R., K. M. Weickmann, and J. E. Kutzbach (1986) Global scale intraseasonal oscillations of outgoing longwave radiation and 250 mb zonal wind during northern hemispheric summer. *Mon. Wea. Rev.*, **114**, 605–623.

Krishnamurthy, V. and R. S. Ajaya Mohan (2010) Composite structure of monsoon low pressure systems and its relation to Indian rainfall. *J. Climate*, **23**, doi: 10.1175/2010JCLI2953.1.

Krishnamurthy, V. and J. Shukla (2000) Intraseasonal and interannual variability of rainfall over India. *J. Climate*, **13**, 4366–4377.

Krishnamurthy, V. and J. Shukla (2001) Observed and model simulated interannual variability of the Indian monsoon. *Mausam*, **52**, 133–150.

Krishnamurthy, V. and J. Shukla (2007) Intraseasonal and seasonally persisting patterns of Indian monsoon rainfall. *J. Climate*, **20**, 3–20.

Krishnamurthy, V. and J. Shukla (2008) Seasonal persistence and propagation of intraseasonal patterns over the Indian monsoon region. *Climate Dynamics*, **30**, 353–369, doi: 10.1007/s00382-007-0300-7.

Krishnamurti, T. N. (1985) Summer monsoon experiment: A review. *Mon. Wea. Rev.*, **113**, 1590–1626.

Krishnamurti, T. N., P. Jayakumar, J. Sheng, N. Surgi, and A. Kumar (1985) Divergent circulations on the 30–50 day time scale. *J. Atmos. Sci.*, **42**, 364–375.

Krishnamurti, T. N., D. Oosterhof, and A. Mehta (1988) Air–sea interactions on the time scale of 30–50 days. *J. Atmos. Sci.*, **45**, 1304–1322.

Krishnamurti, T. N. and P. Ardunay (1980) The 10 to 20 day westward propagating mode and breaks in the monsoons. *Tellus*, **32**, 15–26.

Krishnamurti, T. N. and H. N. Bhalme (1976) Oscillations of monsoon system, Part I: Observational aspects. *J. Atmos. Sci.*, **45**, 1937–1954.

Krishnamurti, T. N. and D. Subrahmanyam (1982) The 30–50 day mode at 850 mb during MONEX. *J. Atmos. Sci.*, **6**(39), 2088–2095.

Krishnan, R., C. Zhang, and M. Sugi (2000) Dynamics of breaks in the Indian summer monsoon. *J. Atmos. Sci.*, **57**, 1354–1372.

Lau, K. M. and P. H. Chen (1986) Aspects of 30–50 day oscillation during summer as inferred from outgoing longwave radiation. *Mon. Wea. Rev.*, **114**, 1354–1369.

Lau, K. M. and L. Peng (1990) Origin of low-frequency (intraseasonal) oscillations in the tropical atmosphere, Part III: Monsoon dynamics. *J. Atmos. Sci.*, **47**(12), 1443–1462.

Lau, K. M., X. Li, and H. T. Wu (2002) Change in the large scale circulation, cloud structure and regional water cycle associated with evolution of the south China Sea monsoon during May–June, 1998. *J. Meteorol. Soc. Japan*, **80**, 1129–1147.

Lau, K. M., M. K. Kim, and K.-M. Kim (2006) Asian summer monsoon anomalies induced by aerosol direct forcing: The role of the Tibetan Plateau. *Climate Dynamics*, **26**, 855–864.

Lau, N. C. (1985) Modelling the seasonal dependence of atmospheric response to observed El Niño in 1962–1976. *Mon. Wea. Rev.*, **113**, 1970–1996.

Lawrence, D. M. and P. J. Webster (2001) Interannual variations of the intraseasonal oscillation in the south Asian summer monsoon region. *J. Climate*, **14**, 2910–2922.

Li, C. and M. Yanai (1996) The onset and interannual variability of the Asian summer monsoon in relation to land–sea thermal contrast. *J. Climate*, **9**, 358–375.

Liebmann, B. and C. A. Smith (1996) Description of a complete (interpolated) out-going longwave radiation dataset. *Bull. Amer. Meteorol. Society*, **77**, 1275–1277.

Liebmann, B., H. H. Hendon, and J. D. Glick (1994) The relationship between tropical cyclones of the western Pacific and Indian oceans and the Madden–Julian Oscillation. *J. Meteorol. Soc. Japan*, **72**, 401–412.

Liu Ping, Y. Kajikawa, Bin Wang, Akio Kitoh, T. Yasunary, Tim Li, H. Annamalai, X. Fu, K. Kikuchi, R. Mizura, K. Rajendran, D. E. Wand, and D. Kim, (2009) Tropical intraseasonal variability in the MRI-20km60L AGCM. *J. Climate*, **22**, 2006–2022.

Madden, R. A. (1986) Seasonal variations of the 40–50 day oscillation in the tropics. *J. Atmos. Sci.*, **43**, 3138–3158.

Madden, R. A. and P. R. Julian (1994) Detection of a 40–50 day oscillation in the zonal wind in the tropical Pacific. *Mon. Wea. Rev.*, **122**, 813–837.

Maloney, E. D. and D. L. Hartmann (2000) Modulation of hurricane activity in the gulf of Mexico by the Madden–Julian Oscillation. *Science*, **287**, 2002–2004.

Manoj, M. G., P. C. S. Devara, P. D. Safai, and B. N. Goswami (2011) Absorbing aerosols facilitate transition of Indian monsoon breaks to active spells. *Climate Dynamics*, doi: 10.1007/s00382-010-0971-3.

Matsuno, T. (1966) Quasi-geostrophic motions in the equatorial area. *J. Meteorol. Soc. Japan*, **44**, 25–43.

Meehl, G. A., J. M. Arblaster, and W. D. Collins (2008) Effects of black carbon aerosols on the Indian monsoon. *J. Climate*, **21**, 2869–2882.

Mooley, D. A. and J. Shukla (1987) *Tracks of Low Pressure Systems which Formed over India, Adjoining Countries, the Bay of Bengal and Arabian Sea in Summer Monsoon Season during the Period 1888–1983*. Center for Ocean Land Atmosphere Studies, Calverton, MD [available from J. Shukla of COLA].

Murakami, M. (1976) Analysis of summer monsoon fluctuations over India. *J. Meteorol. Soc. Japan*, **54**, 15–31.

Murakami, T., T. Nakazawa, and J. He (1984) On the 40–50 day oscillation during 1979 northern hemisphere summer, Part I: Phase propagation. *J. Meteorol. Soc. Japan*, **62**, 440–468.

Murakami, T., L. X. Chen, and A. Xie (1986) Relationship among seasonal cycles, low frequency oscillations and transient disturbances as revealed from outgoing long wave radiation. *Mon. Wea. Rev.*, **114**, 1456–1465.

Nakazawa, T. (1986) Mean features of 30–60 day variations inferred from 8 year OLR data. *J. Meteorol. Soc. Japan*, **64**, 777–786.

Nanjundiah, R. S., J. Srinivasan, and S. Gadgil (1992) Intraseasonal variation of the Indian summer monsoon, Part II: Theoretical aspects. *J. Meteorol. Soc. Japan*, **70**, 529–550.

Pai, D. S., J. Bhate, O. P. Sreejith, and H. R. Hatwar (2009) Impact of MJO on the intraseasonal variation of summer monsoon rainfall over India. *Climate Dynamics*, doi: 10.1007/s00382-009-0634-4.

Pandithurai, G., S. Dipu, K. K. Dani, S. Tiwari, D. S. Bisht, P. C. S. Devara, and R. T. Pinker (2008), Aerosol radiative forcing during dust events over New Delhi, India. *J. Geophys. Res.*, **113**, D1309, doi: 10.1029/2008JD009804.

Parthasarathy, B. and D. Mooley (1978) Some features of a long homogeneous series of Indian summer monsoon rainfall. *Mon. Wea. Rev.*, **106**, 771–781.

Parthasarathy, B., A. Munot, and D. Kothawale (1988) Regression model for estimation of Indian food grain production from Indian summer rainfall. *Agric. For. Meteorol.*, **42**, 167–182.

Pegion, K. and B. Kirtman (2007) The impact of air–sea interactions on the simulation of tropical intraseasonal variability. *J. Climate*, **21**, 6616–6635.

Pearce, R. P. and U. C. Mohanty (1984) Onsets of the Asian summer monsoon, 1979–1982. *J. Atmos. Sci.*, **41**, 1620–1639.

Raghavan, K. (1973) Break-monsoon over India. *Mon. Wea. Rev.*, **101**(1), 33–43.

Rajeevan, M., D. S. Pai, S. K. Dikshit, and R. R. Kelkar (2004) IMD's new operational models for long-range forecast of southwest monsoon rainfall over India and their verification for 2003. *Curr. Sci.*, **86**(3), 422–431.

Rajeevan, M., J. Bhate, J. D. Kale, and B. Lal (2006) High resolution daily gridded rainfall data for the Indian region: Analysis of break and active monsoon spells. *Curr. Sci.*, **91**, 296–306.

Rajeevan, M., S. Gadgil, and J. Bhate (2010) Active and break spells of the Indian summer monsoon. *J. Earth Sys. Sci.*, **119**, 229–248.

Rajendran, K., and A. Kitoh, (2006) Modulation of tropical intraseasonal oscillations by ocean–atmosphere coupling. *J. Climate*, **19**, 366–391.

Rajendran, K., A. Kitoh, and O. Arakawa (2004) Monsoon low frequency intraseasonal oscillation and ocean–atmosphere coupling over the Indian ocean. *Geophys. Res. Lett.*, **31**, doi: 10.1029/2003GL019,031.

Ramage, C. S. (1971) *Monsoon Meteorology* (Vol. 15 of International Geophysics Series). Academic Press, San Diego, CA, 296 pp.

Ramamurthy, K. (1969) *Monsoon of India: Some Aspects of "Break" in the Indian South West Monsoon during July and August* (forecasting manual, Part IV.18.3). India Meteorological Department, New Delhi.

Ramanathan, V. and G. Carmichael (2008) Global and regional climate changes due to black carbon. *Nature Geoscience*, **1**, 221–227.

Ramanathan, V., P. J. Crutzen, J. Lelieveld, A. P. Mitra, D. Althausen, J. Anderson, M. O. Andreae, W. Cantrell, G. R. Cass, C. E. Chung *et al.* (2001) Indian Ocean Experiment: An integrated analysis of the climate forcing and effects of the great Indo-Asian haze. *J. Geophys. Res.*, **106**, 28371–28398, doi: 10.1029/2001JD900133.

Ramanathan, V., Chung, C., Kim, D., Bettge, T., Buja, L., Kiehl, J. T., Washington, W. M., Fu, Q., Sikka, D. R., and Wild, M. (2005) Atmospheric brown clouds: Impacts on South Asian monsoon climate. *Proceedings of the National Academy of Sciences U.S.A.*, **102**(15), 5326–5333.

Ramaswamy, C. (1962) Breaks in the Indian summer monsoon as a phenomenon of interaction between the easterly and the sub-tropical westerly jet streams. *Tellus*, **XIV**, 337–349.

Rao, Y. P. (1976) *Southwest Monsoon* (meteorological monograph). India Meteorological Department, New Delhi, 366 pp.

Reynolds, R. W. and T. M. Smith (1994) Improved global sea surface temperature analyses using optimum interpolation. *J. Climate*, **7**, 929–948.

Sahai, A. K., A. M. Grimm, V. Satyan, and G. B. Pant (2003) Long-lead prediction of Indian summer monsoon rainfall from global SST evolution. *Climate Dynamics*, **20**, 855–863.

Schneider, E. and R. Lindzen (1977) Axially symmetric steady state models of the basic state of instability and climate studies, Part I: Linearized calculations. *J. Atmos. Sci.*, **34**, 263–279.

Sengupta, D. and M. Ravichandran (2001) Oscillations of Bay of Bengal sea surface temperature during the 1998 summer monsoon. *Geophys. Res. Lett.*, **28**(10), 2033–2036.

Sengupta, D., B. N. Goswami, and R. Senan (2001) Coherent intraseasonal oscillations of ocean and atmosphere during the Asian summer monsoon. *Geophys. Res. Lett.*, **28**(21), 4127–4130.

Shukla, J. (1981) Dynamical predictability of monthly means. *J. Atmos. Sci.*, **38**, 2547–2572.

Shukla, J. (1987) Interannual variability of monsoon. In: J. S. Fein and P. L. Stephens (Eds.), *Monsoons*. John Wiley & Sons, New York, pp. 399–464.

Shukla, J. (1998) Predictability in the midst of chaos: A scientific basis for climate forecasting. *Science*, **282**, 728–731.

Sikka, D. R. (1980) Some aspects of large-scale fluctuations of summer monsoon rainfall over India in relation to fluctuations in planetary and regional scale circulation parameters. *Proc. Ind. Acad. Sci. (Earth and Planetary Sciences)*, **89**, 179–195.

Sikka, D. R. and S. Gadgil (1980) On the maximum cloud zone and the ITCZ over Indian longitude during southwest monsoon. *Mon. Wea. Rev.*, **108**, 1840–1853.

Singh, S. V., R. H. Kriplani, and D. R. Sikka (1992) Interannual variability of the Madden–Julian Oscillations in Indian summer monsoon rainfall. *J. Climate*, **5**, 973–979.

Soman, M. and K. Krishna Kumar (1993) Space-time evolution of meteorological features associated with the onset of Indian summer monsoon. *Mon. Wea. Rev.*, **121**, 1177–1194.

Sperber, K. R. and T. N. Palmer (1996) Interannual tropical rainfall variability in general circulation model simulations associated with atmospheric model intercomparison project. *J. Climate*, **9**, 2727–2750.

Sperber K. R., J. M. Slingo, and H. Annamalai (2000) Predictability and the relationship between subseasonal and interannual variability during the Asian summer monsoons. *Quart. J. Roy. Meteorol. Soc.*, **126**, 2545–2574.

Sperber, K. R., C. Brankovic, T. Palmer, M. Deque, C. S. Frederiksen, K. Puri, R. Graham, A. Kitoh, C. Kobayashi, W. Tennant, *et al.* (2001) Dynamical seasonal predictability of the Asian summer monsoon. *Mon. Wea. Rev.*, **129**, 2226–2248.

Srinivasan, J., S. Gadgil, and P. Webster (1993) Meridional propagation of large-scale monsoon convective zones. *Meteorol. Atmos. Phys.*, **52**, 15–35.

Straub, K. and G. Kiladis (2003) Interactions between the boreal summer intraseasonal oscillations and higher-frequency tropical wave activity. *Mon. Wea. Rev.*, **131**, 945–960.

Tomas, R. and P. Webster (1997) The role of inertial instability in determining the location and strength of near-equatorial convection. *Quart. J. Roy. Meteorol. Soc.*, **123**(541), 1445–1482.

Vecchi, G. and D. E. Harrison (2002) Monsoon breaks and subseasonal sea surface temperature variability in the Bay of Bengal. *J. Climate*, **15**, 1485–1493.

Waliser, D. E. and C. Gautier (1993) A satellite-derived climatology of the ITCZ. *J. Climate*, **6**, 2162–2174.

Waliser, D. E., K. Lau, W. Stern, and C. Jones (2003a) Potential predictability of the Madden–Julian Oscillation. *Bull. Amer. Meteorol. Society*, **84**, 33–50.

Waliser, D. E., K. Jin, I.-S. Kang, W. F. Stern, S. D. Schubert, M. L. C. Wu, K.-M. Lau, M.-I. Lee, V. Krishnamurthy, A. Kitoh, *et al.* (2003b) AGCM simulations of intraseasonal variability associated with the Asian summer monsoon. *Climate Dynamics*, doi: 10.1007/s00382-003-0337-1.

Waliser, D. E., R. Murtugudde, and L. Lucas (2004) Indo-Pacific ocean response to atmospheric intraseasonal variability, Part II: Boreal summer and the intraseasonal oscillation. *J. Geophys. Res., Oceans*, **109**, C03030, doi: 10.1029/2003JC002002.

Walker, G. T. (1923) Correlation in seasonal variations of weather, VIII: A preliminary study of world weather. *Mem. Indian Meteorol. Dept.*, **24**, 75–131.

Walker, G. T. (1924) Correlation in seasonal variations of weather, IV: A further study of world weather. *Mem. Indian Meteorol. Dept.*, **24**, 275–332.

Wang, B. and H. Rui (1990) Synoptic climatology of transient tropical intraseasonal convection anomalies: 1975–1985. *Meteorol. Atmos. Phys.*, **44**, 43–61.

Wang, B. and X. Xie (1997) A model for the boreal summer intraseasonal oscillation. *J. Atmos. Sci.*, **54**(1), 71–86.

Wang, B., I.-S. Kang, and J.-Y. Lee (2004) Ensemble simulations of Asian–Australian monsoon variability by 11 AGCMs. *J. Climate*, **17**, 699–710.

Webster, P. J. (1983) Mechanism of monsoon low-frequency variability: Surface hydrological effects. *J. Atmos. Sci.*, **40**, 2110–2124.

Webster, P. J. and C. Hoyos (2004) Prediction of monsoon rainfall and river discharge on 15–30 day time scales. *Bull. Amer. Meteorol. Society*, **85**, 1745–1767.

Webster, P. J., V. O. Magana, T. N. Palmer, J. Shukla, R. T. Tomas, M. Yanai, and T. Yasunari (1998) Monsoons: Processes, predictability and the prospects of prediction. *J. Geophys. Res.*, **103**(C7), 14451–14510.

Webster, P. J., E. F. Bradley, C. W. Fairall, J. S. Godfrey, P. Hacker, R. A. Houze Jr., R. Lukas, Y. Serra, J. M. Hummon, T. D. M. Lawrence *et al.* (2002) The JASMINE pilot study. *Bull. Amer. Meteorol. Society*, **83**(11), 1603–1630.

Wentz, F., C. Gentemann, D. Smith, and D. Chelton (2000) Satellite measurements of sea surface temperature through clouds. *Science*, **288**, 847–850.

Wheeler, M. C. and H. H. Hendon (2004) An all-season real-time multivariate MJO Index: Development of an index for monitoring and prediction. *Mon. Wea. Rev.*, **132**, 1917–1932.

Wheeler, M. C. and G. N. Kiladis (1999) Convectively coupled equatorial waves: Analysis of clouds and temperature in the wavenumber–frequency domain. *J. Atmos. Sci.*, **56**, 374–399.

Wu, M., S. Schubert, I.-S. Kang, and D. Waliser (2002) Forced and free intraseasonal variability over the south Asian monsoon region simulated by 10 AGCMs. *J. Climate*, **15**(20), 2862–2880.

Xavier, P. K. and B. N. Goswami, (2007) An analog method for real time forecasting of summer monsoon subseasonal variability. *Mon. Wea. Rev.*, **135**, 4149–4160.

Xie, P. and P. A. Arkin (1996) Analyses of global monthly precipitation using gauge observations, satellite estimates and numerical predictions. *J. Climate*, **9**, 840–858.

Yanai, M. and T. Tomita (1998) Seasonal and interannual variability of atmospheric heat sources and moisture sinks as determined from NCEP–NCAR reanalysis. *J. Climate*, **11**, 463–482.

Yasunari, T. (1979) Cloudiness fluctuation associated with the northern hemisphere summer monsoon. *J. Meteorol. Soc. Japan*, **57**, 227–242.

Yasunari, T. (1980) A quasi-stationary appearance of 30–40 day period in the cloudiness fluctuation during summer monsoon over India. *J. Meteorol. Soc. Japan*, **58**, 225–229.

Yasunari, T. (1981) Structure of an Indian summer monsoon system with around 40-day period. *J. Meteorol. Soc. Japan*, **59**, 336–354.

Zheng, Y., D. E. Waliser, W. Stern, and C. Jones (2004) The role of coupled sea surface temperatures in the simulation of the tropical intraseasonal oscillation. *J. Climate*, **17**(21), 4109–4134.

http://www.springer.com/978-3-642-13913-0

Intraseasonal Variability in the Atmosphere-Ocean Climate System

Lau, W.K.-M.; Waliser, D.E.

2012, XXXIV, 614 p., Hardcover
ISBN: 978-3-642-13913-0